International Atomic Energy Agency

INDC(CCP)-353
Distr.: G

INDC INTERNATIONAL NUCLEAR DATA COMMITTEE

LECTURES PRESENTED AT THE INTERREGIONAL TRAINING COURSE ON APPLICATION OF NUCLEAR DATA AND MEASUREMENT TECHNIQUES IN NUCLEAR REACTOR AND PERSONAL NEUTRON DOSIMETRY

Obninsk, The Russian Federation
15 June to 10 July 1992

April 1993

IAEA NUCLEAR DATA SECTION, WAGRAMERSTRASSE 5, A-1400 VIENNA

INDC(CCP)-353
Distr.: G

LECTURES PRESENTED AT THE INTERREGIONAL TRAINING COURSE ON APPLICATION OF NUCLEAR DATA AND MEASUREMENT TECHNIQUES IN NUCLEAR REACTOR AND PERSONAL NEUTRON DOSIMETRY

Obninsk, The Russian Federation
15 June to 10 July 1992

April 1993

Reproduced by the IAEA in Austria
April 1993
93-01215

CONTENTS

TESTING CAPTURE CROSS-SECTIONS OF FISSION PRODUCTS IN REACTIVITY PERTURBATION EXPERIMENTS

S.M.Bednyakov, G.N.Manturov (IPPE, Obninsk)
K.Dietze (ZfK, Dresden)

ABSTRACT

Central reactivity worths for twelve fission product nuclides ($^{95,97,98,100}Mo$, ^{103}Rh, ^{105}Pd, ^{141}Pr, $^{143,145}Nd$, ^{149}Sm, ^{153}Eu) were measured on 15 fast critical assemblies. The measured central reactivity worths normalized by ^{10}B were compared with calculational values. Necessary corrections (on heterogeneity of media, self-shielding of media and that of a sample and others) were introduced to ensure adequate conditions for the comparison. The IPPE recommended library of fission product capture cross-sections was tested by this comparison and some corrections to these cross-sections were proposed. A satisfactory agreement of the obtained experimental data with STEK and CFRMF experiments was observed in case of similar conditions. The evaluated experimental information was used for updating БНАБ group cross-section library (БНАБ-90).

INTRODUCTION

In 1983-1988 in the Institute of Physics and Power Engineering (IPPE, Obninsk) the experiments were carried out on a series of fast critical assemblies to test capture cross-sections of most important stable fission products(FP) accumulated in a fast reactor core.

On the whole 15 cores with dioxide and metallic fuel (both U and U-Pu) were investigated. The spectral range of assemblies included all fast reactor types of possible interest. Most of the experiments were carried out on БФС facility, some of them - on КБР facility and one of the experiments on - SEG facility (Zfk,Dresden).

Central reactivity worths (CRW) of FP samples were measured by a periodical criticality perturbation method. A list of investigated FPs' and their contributions into a total absorbtion of all fission products is given in Table 1 according to /1/. The investigated nuclides are responsible for approximately 36% of the total FPs' absorbtion.

DESCRIPTION OF THE INVESTIGATED ASSEMBLIES

БФС and КБР critical assemblies consist of tightly packed vertical stainless steel tubes arranged to a triangle lattice. The tubes were filled with pellets of fuel and other materials. The

Table 1

The contribution of investigated nuclides to total absorbtion of fission products for БН-1600 spectrum.

Nuclide	Contribution,%	Nuclide	Contribution,%
^{95}Mo	1.5	^{109}Ag	2.7
^{97}Mo	2.9	^{141}Pr	0.9
^{98}Mo	1.2	^{143}Nd	2.3
^{100}Mo	0.9	^{145}Nd	3.4
^{103}Rh	5.5	^{149}Sm	3.4
^{105}Pd	9.9	^{153}Eu	1.3

outer diameter of the tube is 50 mm, the wall thickness is 1 mm, the lattice pitch is 51 mm.

The structure of the SEG assembly was similar to that of БФС assemblies. Pellets of the same size were placed into vertical channels arranged in an aluminium block with the same lattice pitch.

More detailed description of the assemblies is given in /2,3/. A homogeneous concentrations of core materials are presented in Table 2. Some characteristics of investigated critical assemblies are given in Table 3.

The CRW measurements were carried out in the intertube gaps near the central tube of БФС and КБР cores and in the special graphite column in the center of SEG.

CALCULATION APPROACH AND ANALYSIS OF EXPERIMENTAL RESULTS

The measured CRW of FPs (marked below as ρ^1) were normalized by CRW of ^{10}B (ρ^{10}), whose absorbtion cross-section is well known and depends on the energy according to 1/v law.

An energy dependence of capture cross-sections for most of the FPs in the investigated energy range is similar to that of ^{10}B. That is why the use of boron as a standard for interpretation of reactivity measurement results allows to exclude some of systematic errors arising in the calculational procedure of heterogeneous corrections, corrections on spectrum and self-shielding factors perturbation et al.

A one-dimensional spherical model for a calculation of the critical assemblies was used. The calculations of assemblies were carried out by КРАБ-1 code /4/ using P_1- and S_n-approximations with

Table 2

Homogeneous concentrations of elements in the assemblies
($*10^{22}$ nucl./cm^2).

Assembly	^{235}U	^{238}U	^{239}Pu	O	Na	Fe	Cr
БФС-45А-1	0.182	0.668	0	1.299	0.768	1.045	0.287
БФС-45Б-1	0.181	0.668	0	1.715	0.785	1.328	0.338
БФС-47-5	0.003	0.624	0.170	1.254	0.741	1.153	0.318
БФС-49-1	0.005	1.263	0.172	2.537	0	0.558	0.149
БФС-49-2	0.004	0.969	0.132	1.948	0	0.525	0.141
БФС-49-3	0.005	1.250	0.169	2.512	0	0.559	0.143
БФС-49-4	0.004	0.966	0.131	1.940	0.382	0.629	0.171
БФС-51-1	0.379	0.661	0	0	1.000	1.120	0.305
БФС-52-1	0.197	0.690	0	1.354	0.517	1.362	0.375
БФС-55-1	0.005	1.274	0.142	0	0.621	1.652	0.459
КБР-10	0.048	0.006	0	0.110	0	4.480	1.247
КБР-12	0.051	0.265	0	0.634	0	3.816	1.524
КБР-13	0.049	0.206	0	0.521	0	0.722	4.024
КБР-15	0.026	0.003	0	0.059	0	0.454	5.246
SEG-V	0.173	0.307	0	0	0	0	0
БФС-45А-1	0.134	0.271	0.023	0.038	0.011	0.002	0
БФС-45Б-1	0.246	0	0	0	0	0	0
БФС-47-5	0.149	0.222	0.025	0.038	0.012	0.001	0.007
БФС-49-1	0.070	0.414	0.012	0.064	0.006	0.001	0.007
БФС-49-2	0.066	0.320	0.011	1.494	0.005	0.001	0.005
БФС-49-3	0.075	0.399	0.011	0.128	0.005	0.123	0.008
БФС-49-4	0.080	0.319	0.013	0.050	0.006	0.001	0.005
БФС-51-1	0.143	0.328	0.024	0.007	0.011	0	0
БФС-52-1	0.175	0.697	0.030	0.026	0	0	0
БФС-55-1	0.215	0.204	0.036	0.037	0.017	0.001	0.006
КБР-10	0.583	0	0.098	0.151	0	0	0.163
КБР-12	0.064	0.102	0.011	0.016	0.005	0	0
КБР-13	0.094	0.048	0.016	0.005	0.008	0	0
КБР-15	0.059	0.015	0.010	0.003	0	0	0
SEG-V	0	1.381	0	5.608	0	0	0.159

Notes: *) R - for БФС ^{240}Pu
- for КБР Mo-nat.
- for SEG B-nat.

Table 3

Some integral parameters of assemblies.

Assembly	Fuel	Enrich-ment,%	Share of neutrons in spectrum with $E_n \leq 10$ keV,%	ρ^{10}/ρ^{235} calc. ($*10^{-2}$)	ρ^{1}/ρ^{235} exp. ($*10^{-3}$)
БФС-45А-1	UO_2	21	4.7	-110	175 ± 3
БФС-45Б-1	UO_2	21	5.3	-110	213 ± 3
БФС-47-5	$(PuU)O_2$	21	4.2	- 88	55 ± 2
БФС-49-1	$(PuU)O_2$	12	5.4	- 66	- 2 ± 1
БФС-49-2	$(PuU)O_2$	12	13.1	- 92	77 ± 1
БФС-49-3	$(PuU)O_2$	12	11.3	-102	42 ± 1
БФС-49-4	$(PuU)O_2$	12	6.7	- 72	24 ± 1
БФС-51-1	U	36	0.4	- 72	316 ± 3
БФС-52-1	UO_2	22	4.6	-110	250 ± 5
БФС-55-1	PuU	10	2.4	- 60	- 93 ± 2
КБР-10	UO_2	90	16.0	-154	----
КБР-12	UO_2	16	15.1	-135	----
КБР-13	UO_2	19	13.0	-129	- 15 ± 1
КБР-15	UO_2	90	16.7	-185	----
SEG-V	U	36	18.4	-162	- 4 ± 1
STEK-500	U	90	6.2	-146	----
STEK-1000	U	90	13.5	-253	----
STEK-2000	U	90	18.5	-348	----
CFRMF	U	93	7.8	108*)	----

Notes: 1. *) σ^{10}/σ^{235} - absorbtion to fission cross-sections ratio;
2. ρ^{1}, ρ^{10}, ρ^{235} - central reactivity worths of hydrogen, ^{10}B and ^{235}U correspondingly.

АРАМАКО-80 26-group constants preparation on the basis of БНАБ-78 nuclear data library /5/. During FPs CRW calculation the group cross-sections and self-shielding factors were used after deriving from evaluated neutron data files prepared in the IPPE /6/ and condensing into group constants by means of ГРУКОН code /7/.

A heterogeneous structure of assemblies was taken into account by means of a cell code НЕЕРС /8/. A neutron and adjoint flux in a flat layers model of real cell were calculated by the first collision probability method using the integral transport approximation with resonance self-shielding calculations procedure proposed by T.Tone /9/. A self-shielding for samples of different thickness used in the experiments was assessed by the rational Wigner approxi-

Table 4

Description of samples for reactivity perturbation.

Material	Main isotope content,%	Material	Main isotope content,%
^{95}Mo	95.4	^{109}Ag	99.4
^{97}Mo	91.7	85% $^{141}PrO_2$ +	
		+15% $^{141}Pr_2O_3$	100
^{98}Mo	95.9	$^{143}Nd_2O_3$	83.2
^{100}Mo	96.1	$^{145}Nd_2O_3$	84.8
^{103}Rh	100	$^{149}Sm_2O_3$	96.9
^{105}Pd	93.8	$^{153}Eu_2O_3$	99.2

mation /10/. A bilinear corrections which are understood as resonance self-shielding decrease in the surrounding medium due to neutron scattering in the sample were also made. The uncertainties of the heterogeneity and sample self-shielding corrections were also evaluated experimentally. They are given in this paper together with the statistical ones.

EXPERIMENTAL SAMPLES

Samples of FPs and ^{10}B used in the experiments were of different thicknesses. Types of chemical compounds of investigated nuclides and contents of the main isotopes are given in Table 4. The contribution of oxygen to a sample worth was measured by means of Al and Al_2O_3 samples. The influence of isotopic admixtures in samples was calculated. The worth of stainless steel cladding of the samples was measured in an additional experiment.

At a preliminary stage during comparing the experimental and calculational ratios of CRW $r^i=\rho^i/\rho^{10}$ for some FPs ($^{95,97,98}Mo$, ^{141}Pr, $^{143,145}Nd$, ^{149}Sm) an essential scattering of discrepancies between experiments and calculations $\delta^i=(r_e^i-r_c^i)*100/r_e^i$ was observed in assemblies with similar spectra (a spectrum characteristic in this paper, ε - is a share in the spectrum of neutrons with energy below 10 keV).

A hypothesis of moisture presence in some samples was proposed for explanation of this fact. The main reasons for taking this hypothesis into consideration were smooth dependence of δ^i on ε and absence of δ^i dependence on hydrogen to ^{235}U CRW ratio (ρ^1/ρ^{235}). A further analysis of measured CRW ratios and an additional

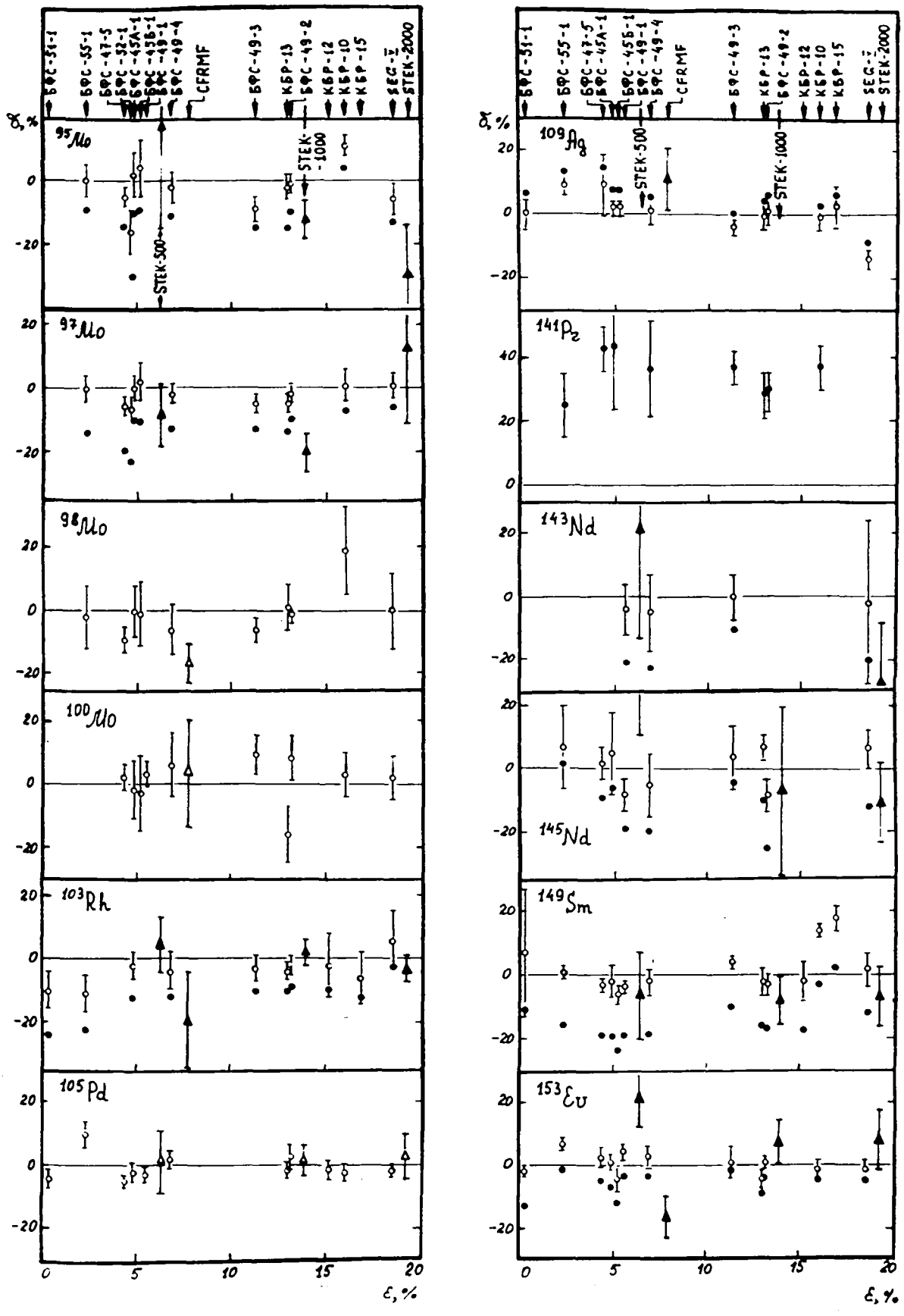

Fig. 1. Discrepancies δ^i between experimental and calculational ρ^i/ρ^{10} values.

experimental information on ratios of hydrogen and oxygen CRW to ^{235}U one (ρ^1/ρ^{235} and ρ^{16}/ρ^{235}) for entire set of assemblies allowed to confirm this hypothesis, to determine a mass content of moisture in the samples and introduce necessary corrections to the experimental ρ^i/ρ^{235} ratios. The control points for this assessment were the experimental data obtained on the assemblies with with $\rho^1/\rho^{235} \simeq 0$ and with essentially different ε (SEG-V and БФС-49-1). The reliability criterion of moisture content determination in the samples can be an agreement of the results obtained with "wet" IPPE samples of ^{149}Sm and "dry" ZfK ones /12/. This method of moisture determination was confirmed by a patent of the Federal Republic of Germany /13/.

COMPARISON OF EXPERIMENTS AND CALCULATIONS. CROSS-SECTIONS CORRECTION.

In addition to comparison of experimental data from БФС, КБР and SEG with calculational ones on the basis of evaluated data files /6/ capture cross-sections correction of FPs was carried out. The capture cross-sections for a number of FP nuclides were corrected to provide their agreement with the experimental data from БФС, КБР and SEG assemblies. An attention was paid to avoid contradictions with existing differential measurements of capture cross-sections.

The extent of agreement between measured ρ^i/ρ^{10} and those calculated on the basis of data recommended in /6/ as well as corrected capture cross-sections are shown in Figure 1.

The energy dependences of FP capture cross-sections resulting from different evaluations including those proposed in this paper are shown in Figures 2-11.

The general information on the results of FPs capture cross-sections testing is given in Table 5. The discrepancies between calculated and measured values of ρ^i/ρ^{10} are presented as an average discrepancy for entire set of assemblies: $\delta^i=(1/N)\sum\delta^i_n$ (N is a number of investigated assemblies).

Values of proposed cross-section correction can be found both from Figures 2-11 and in the last coloumn of the Table 5 (j is the energy group number in 26 - group approximation).

The evaluated uncertainties of tested and corrected capture cross-sections of investigated nuclides are given in Table 6. It should be noted that more detailed analysis of the obtained integral data was carried out in papers /12,22,23/.

The experiments on criticality perturbation of assemblies by a small samples were carried out earlier in Netherlands (STEK), Sweden

Table 5

Capture cross-sections testing for fission products on a fast critical assemblies.

Nuclide	Version /6/	Average uncertainty of capture cross-section %	Number of investigated assemblies	Discrepancy δ^1,% in comparison with		Recommendations on correction of version /6/
				version /6/	correction result	
^{95}Mo	JENDL-2	15	11	-13 ± 3	-3 ± 2	-(10-18)% j=6-13
^{97}Mo	JENDL-2	15	11	-13 ± 2	-2 ± 1	-(8-26)% j=6-12
^{98}Mo	JENDL-2	20	10	- 2 ± 3	-2 ± 3	JENDL-2
^{100}Mo	JENDL-2	20	10	+ 1 ± 2	+1 ± 2	JENDL-2
^{103}Rh	IPPE	15	10	-12 ± 2	-4 ± 1	-(5-23)% j=3-14
^{105}Pd	IPPE	10	11	- 1 ± 1	-1 ± 1	IPPE
^{109}Ag	IPPE	10	12	+ 5 ± 2	+1 ± 2	+(2-14)% j=6-14
^{141}Pr	ENDF/B4	10	8	+36 ± 2	----	contradicts to differ. data
^{143}Nd	IPPE	20	4	-18 ± 3	-3 ± 1	+(5-28)% j=6,7,15 -(3-17)% j=8-14
^{145}Nd	IPPE	20	9	-12 ± 3	+1 ± 2	+(1-17)% j=6-8 -(0-26)% j=9-15
^{149}Sm	IPPE	20	14	-14 ± 2	+2 ± 2	JENDL-1
^{153}Eu	ENDF/B4	15	12	- 6 ± 1	+1 ± 1	-(2-11)% j=6-14

Table 6

The evaluated uncertainties of fission products capture cross-sections as the result of testing.

Nuclide	Energy range (keV)		
	1 - 100	100 - 800	800 - 1400
^{95}Mo	5	8	15
^{97}Mo	6	12	20
^{98}Mo	4	6	10
^{100}Mo	3	5	8
^{103}Rh	4	9	15
^{105}Pd	4	6	15
^{109}Ag	3	6	10
^{143}Nd	10	10	15
^{145}Nd	10	10	15
^{149}Sm	7	7	10
^{153}Eu	3	5	8

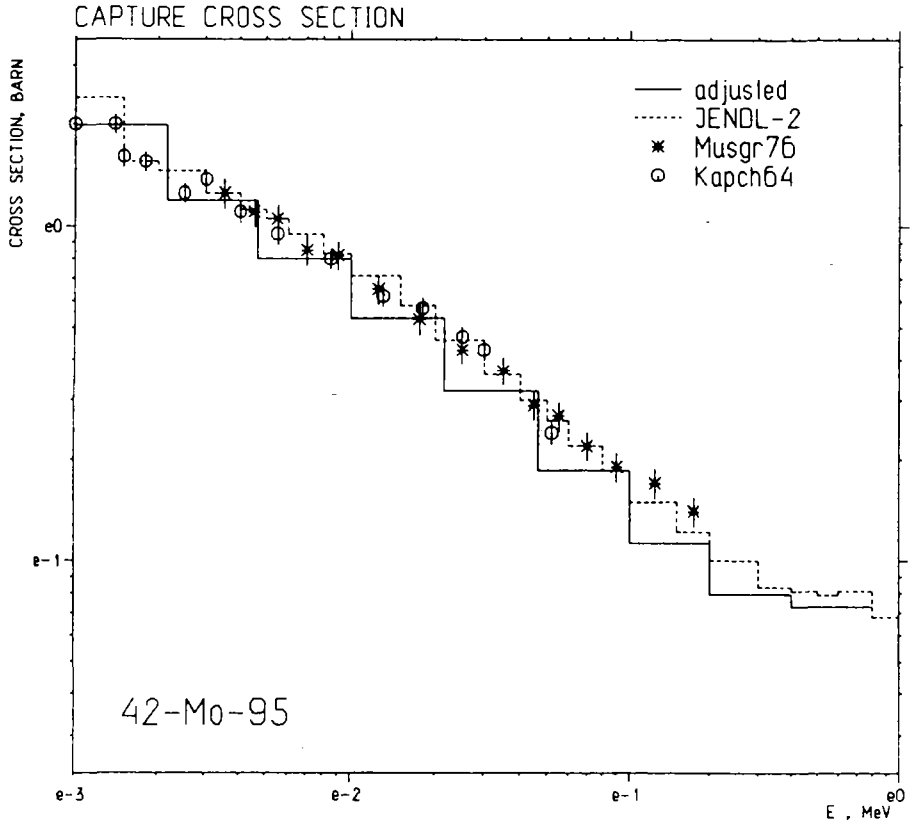

Fig.2. A radiative capture cross section of the molybdenum-95.

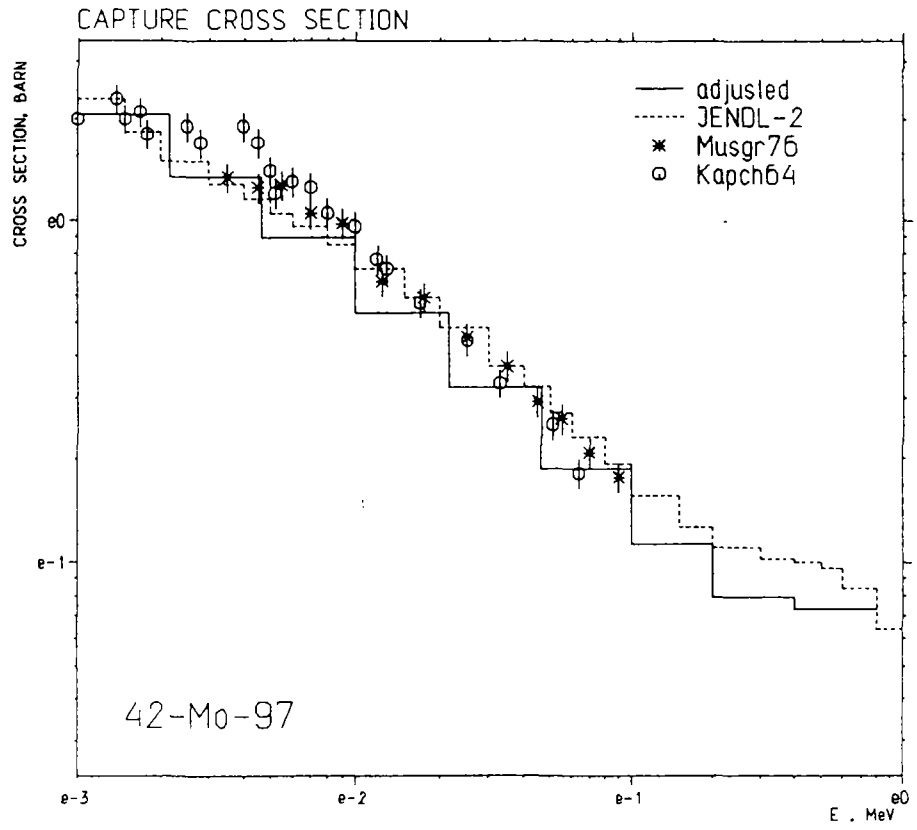

Fig.3. A radiative capture cross section of the molybdenum-97.

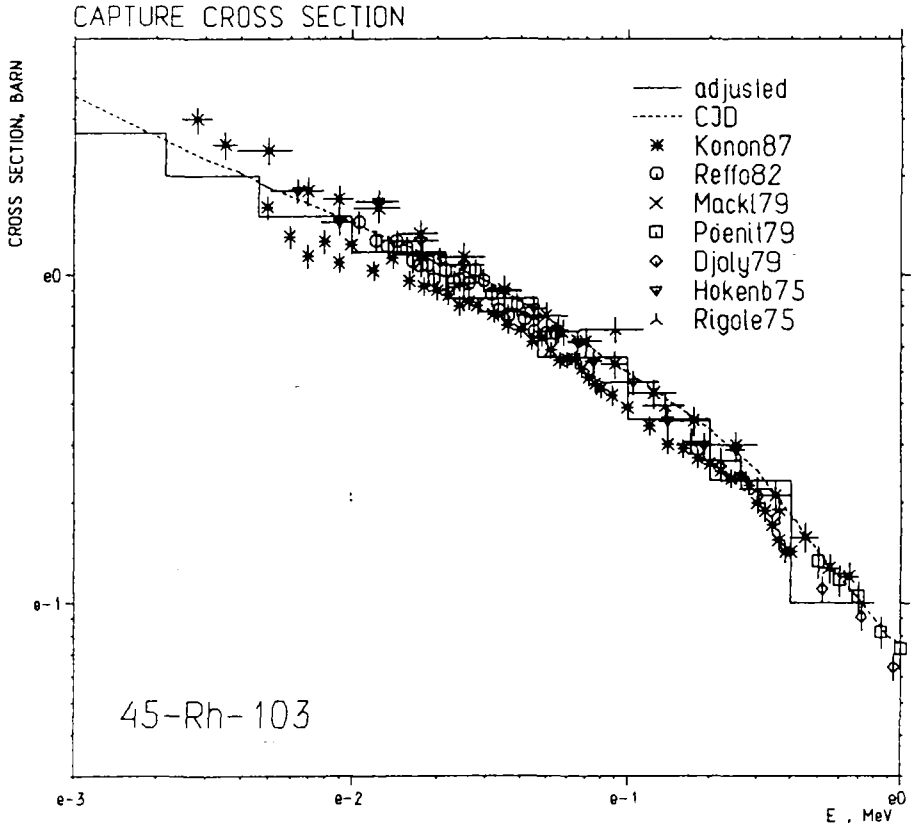

Fig.4.A radiative capture cross section of the rhodium-103.

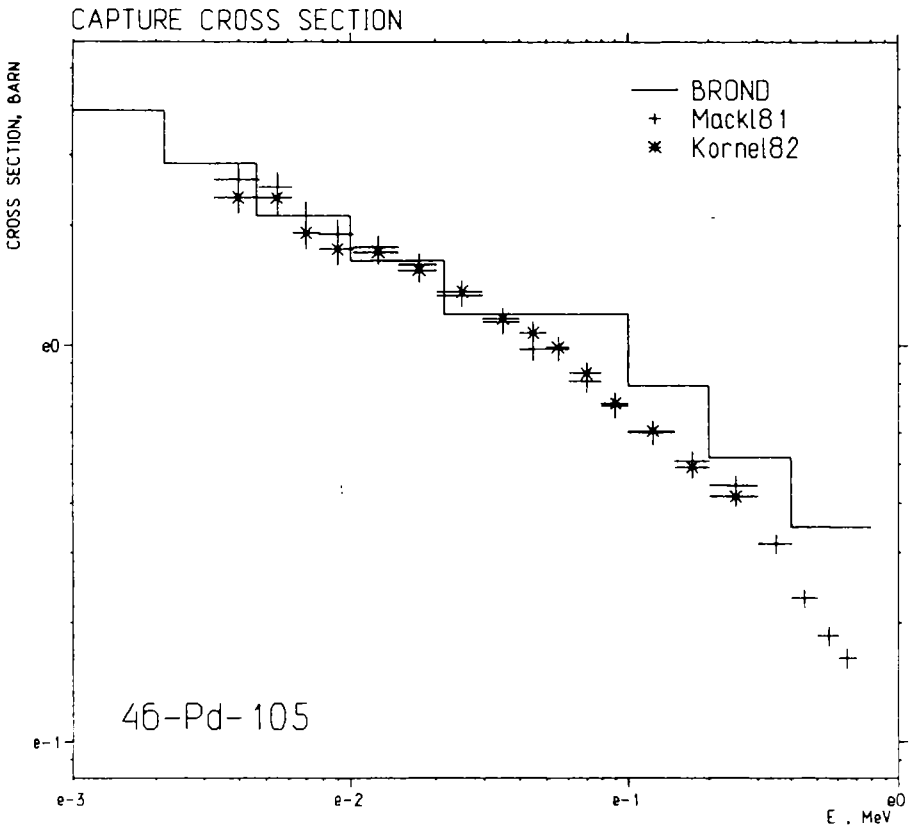

Fig.5. A radiative capture cross section of the palladium-105.

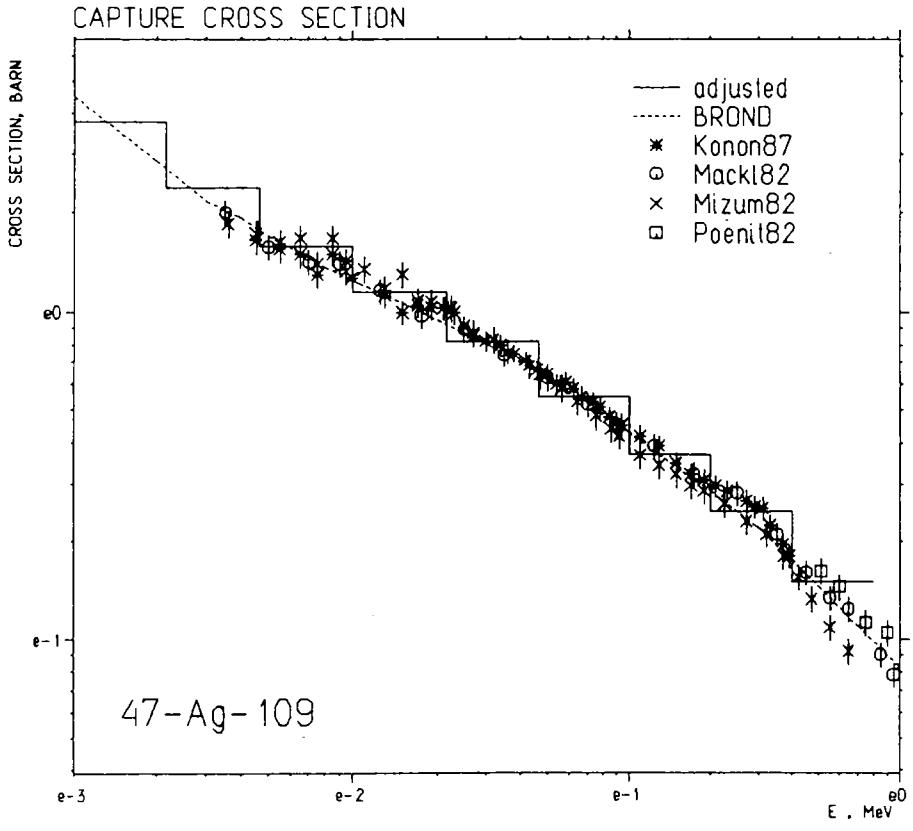

Fig.6. A radiative capture cross section of the silver-109.

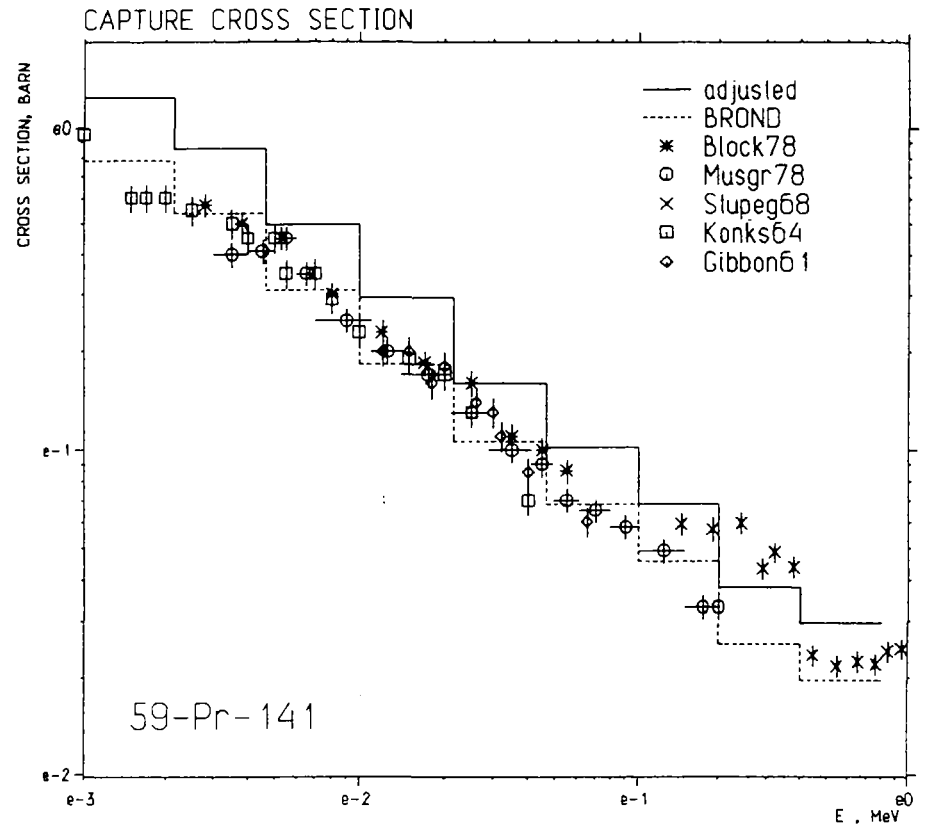

Fig.7. A radiative capture cross section of the praseodymium-141.

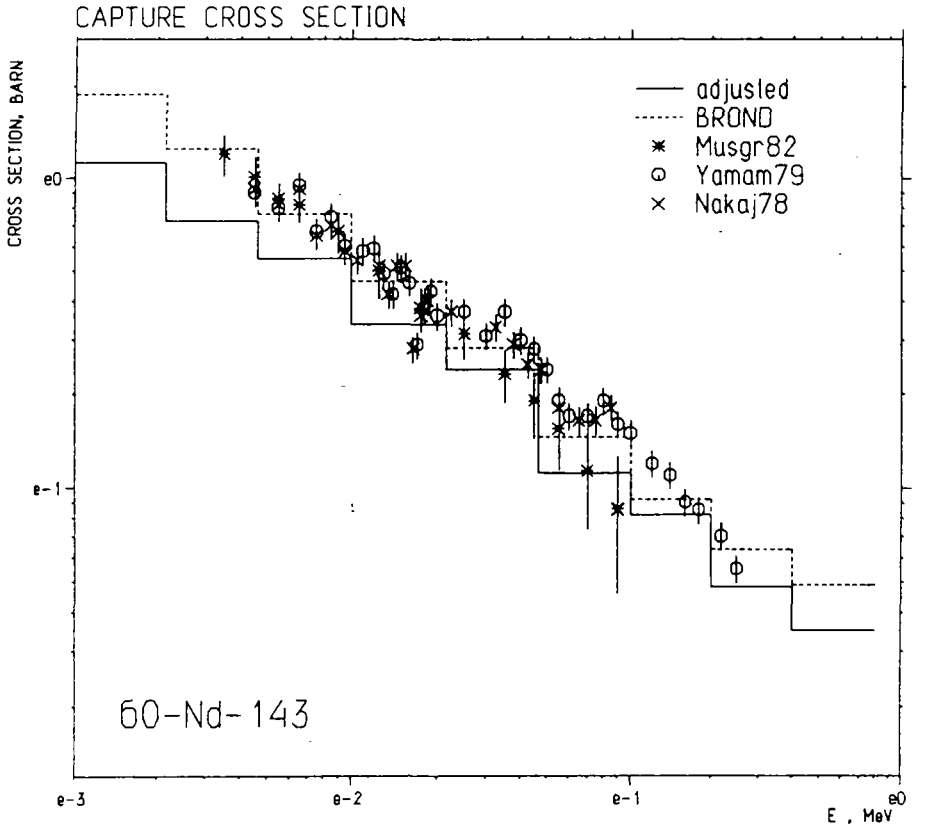

Fig.8. A radiative capture cross section of the neodymium-143.

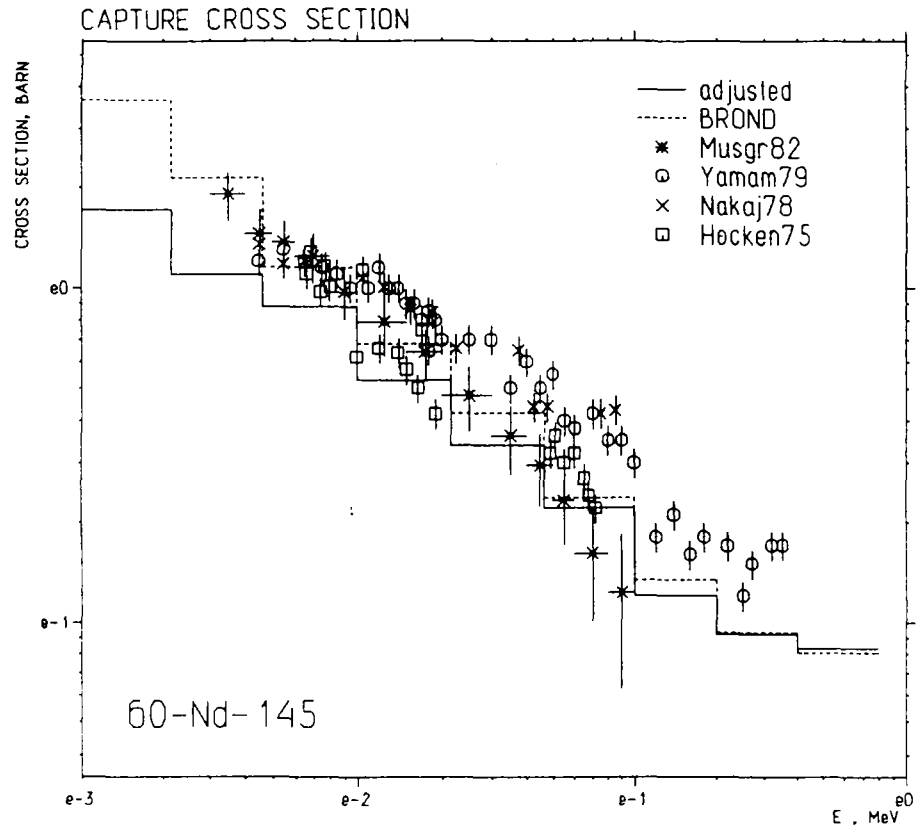

Fig.9. A radiative capture cross section of neodymium-145.

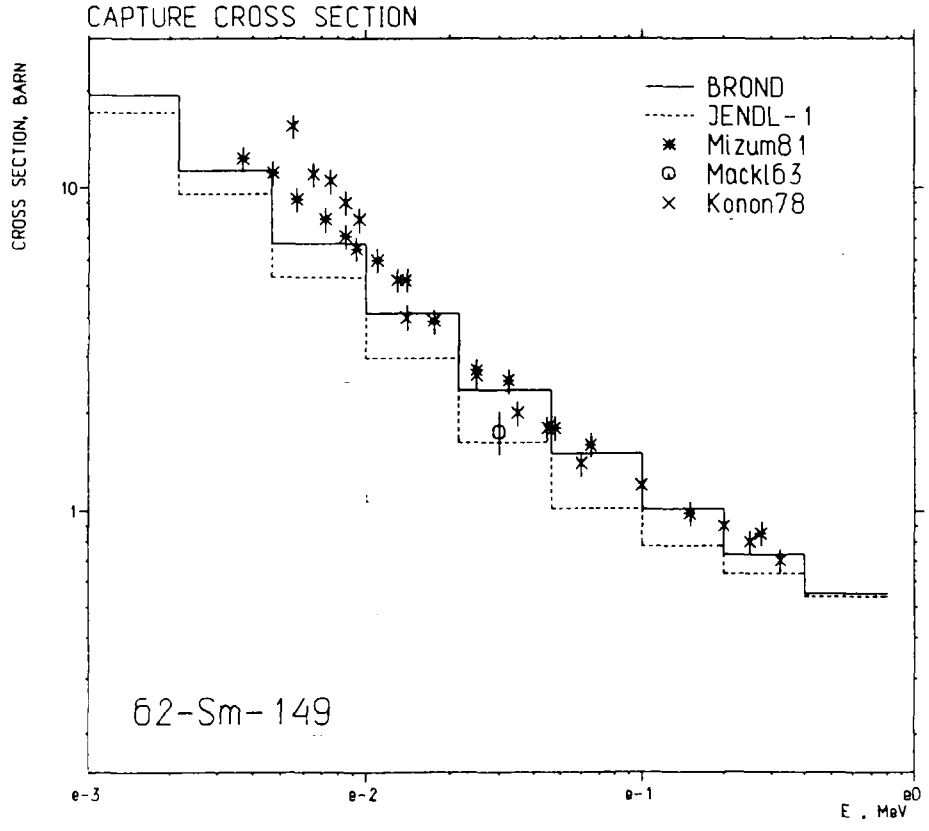

Fig.10. A radiative capture cross section of the samarium-149.

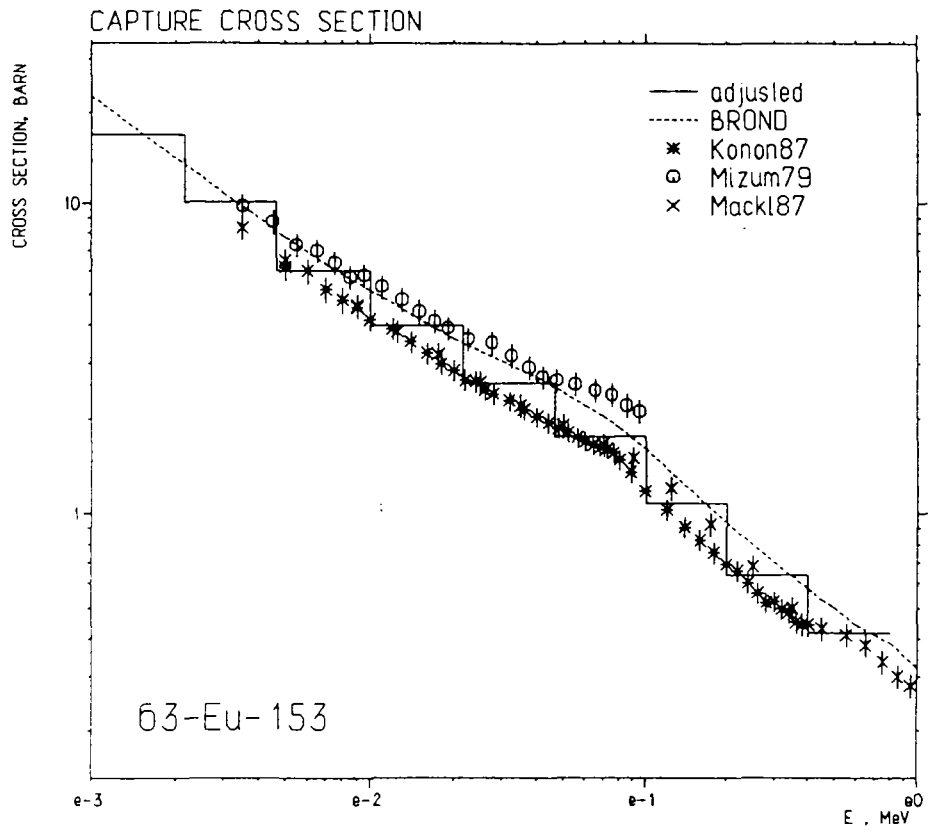

Fig.11. A radiative capture cross section of the europium-153.

(FRO), France (ERMINE, MASURCA) /14-20/. Moreover, the average capture cross-sections of FPs were measured in USA on CFRMF assembly by activation method /21/.

It was of interest to compare the results of БФС, КБР and SEG measurements with other ones. Unfortunately, we have not enough information about experiments on FRO, ERMINE and MASURCA. Nonetheless, the comparison proved to be possible with STEK and CFRMF data.

The structure of STEK could be easily presented by the flat layers model like БФС, КБР and SEG. This fact allowed to use our calculational methods for assessment of experiments on these assemblies. Spectral characteristic ε (a share of neutrons in the spectrum with energy below 10 keV) for STEK assemblies covers the entire range of БФС, КБР and SEG assemblies. But the most suitable cores from the point of view of comparison with our results are STEK-500, -1000 and -2000 whose spectrum is harder then that of other STEK cores. It is also true for CFRMF assembly. Some integral parameters of these assemblies are also given in Table 3.

The agreement of STEK, CFRMF, БФС, КБР and SEG results can be demonstrated by Figure 1.

Since for obtaining corrected cross-sections only the integral data of this paper were used the comparison of STEK and CFRMF

results in Figure 1 is only made with evaluated data /6/ that is enough for assessment of the experimental data agreement.

CONCLUSIONS

The FP capture cross-sections testing on the basis of results from the experiments on БФС, КБР and SEG critical assemblies allowed to improve essentially the reliability and accuracy of the neutron data. No corrections are required for the capture cross-sections of even molibdenium isotopes because of good agreement of experimental and calculational CRW. For ^{141}Pr the data of CRW measurements require to increase capture cross-sections in the region of 1 keV - - 1 MeV by about 50-60%. This contradicts essentially with recommendation made on the basis of differential measurements. So, we do not propose any corrections for this isotope.

The agreement of STEK and CFRMF data with results of this paper in most cases can be considered to be satisfactory.

The evaluated experimental information about capture cross--sections of the investigated nuclides was documented and included in the computer library of macroexperiments LEMEX /24/. This information together with the results of testing recent versions of neutron data for reactor materials was used for updating БНАБ group cross-section library (БНАБ-90).

REFFERENCES

1. Schenter R.,England T. ENDF/B-5 Fission product cross--section evaluation.-In: Proc. Spec. Meeting on Neutron Cross--Sections of Fission Product Nuclei. 1979, Bologna, Italy; NEANDC(E), 209"L", p.253.

2. Казанский Ю.А.,Дулин В.А.,Зиновьев В.П. и др. Методы изучения реакторных характеристик на критических сборках БФС. М.: томиздат, 1977.

3. Dietze K.,Fahrmann K.,Huttel G.,Lehmann E. Neutron data check for structural materials by reactivity measurements in a fast facility with energy independent adjoint flux.- Kernenergie, 1986, Bd 29, s.401.

4. Савоськин М.М.,Маркелов И.П.,Барыба М.А. и др. Аннотация пакета программ КРАБ-1. -Вопросы атомной науки и техники. Сер.: Физика и методы расчета ядерных реакторов, 1984, вып.6(43), с.44.

5. Абагян Л.П.,Базазянц Н.О.,Николаев М.Н.,Цибуля А.М. Групповые константы для расчета реакторов и защиты. М.: Энергоиздат, 1981.

6. Игнатюк А.В.,Кравченко И.В.,Мантуров Г.Н. Библиотека рекомендованных оцененных нейтронных сечений для важнейших продуктов деления ядер. -Вопросы атомной науки и техники. Сер.: Ядерные константы. 1987, вып.1, с.3.

7. Синица В.В. Программа расчета групповых констант на основе библиотек оцененных нейтронных данных. -Вопросы атомной науки и техники. Сер.: Ядерные константы, 1984, вып.5(59), с.34.

8. Бедняков С.М. Реализация метода оценки интегральных экспериментов в условиях стенда БФС: Препринт ФЭИ-2114, 1990.

9. T.Tone. -Journal on Nuclear Science and Technology, -1975, v.12, p.467.

10. Белл Д.,Глесстон С. Теория ядерных реакторов. Пер. с англ. под ред. В.Н.Артамкина - М.: Атомиздат, 1974.

11. Дулин В.А. Оценка точности групповых расчетов возмущений критичности реакторов. -Вопросы атомной науки и техники. Сер.: Ядерные константы, 1983, вып.1(50), с.63.

12. Бедняков С.М.,Мантуров Г.Н.,Дитце К. Тестировка сечений захвата некоторых лантаноидов-продуктов деления в экспериментах на быстрых критсборках. -Вопросы атомной науки и техники. Сер.: Ядерные константы, 1990, вып.4, с.91.

13. E. Lehmann,G.Huttel,K.Dietze,S.M.Bednyakov.- Patentschrift DD 294098 A5.

14. Klippel H.,Smith J. The coupled fast-thermal critical facility STEK.- RCN-209, 1974.

15. Veenema J.,Janssen A. Small sample reactivity worths of fission product isotopes and some other materials measured in STEK.-- ECN-10, 1976.

16. Fast Reactor Programme Second Quarter 1973 Progress Report.- RCN-190, 1973.

17. Fast Reactor Programme Third Quarter 1973 Progress Report.-- RCN-199, 1973.

18. Fast Reactor Programme Fourth Quarter 1973 Progress Report.- RCN-207, 1974.

19. Anderson T. Integral measurements of fission product reactivity worths in some fast reactor spectra.- AE-428, 1971.

20. Martin-Deidier L. Mesure integrale de la capture des produits de fission dans les reacteurs a neutron rapides. CEA-R--5023, 1979.

21. Harker Y.,Anderl R. Integral cross-sections measurements on fission products nuclides in fast reactor fields.- In: Proc. Spec. Meet. on Neutron Cross-Sections of Fission Product Nuclei, Bologna, Italy, Dec. 12-14, 1979, p.5.

22. Бедняков С.М.,Боховко М.В.,Мантуров Г.Н.,Дитце К. Уточнение сечений захвата ^{103}Rh, ^{105}Pd, ^{109}Ag и ^{153}Eu на основе анализа экспериментов на быстрых сборках. -Атомная энергия, 1989, т.67, вып.3, с.199.

23. Бедняков С.М.,Мантуров Г.Н.,Дитце К. Уточнение сечений захвата изотопов молибдена на основе анализа экспериментов на быстрых сборках. -Атомная энергия, 1990, т.69, вып.1, с.31.

24. Коробейникова Л.В.,Мантуров Г.Н.,Цибуля А.М. Библиотека оцененных макроскопических экспериментов на быстрых критсборках и реакторах. -В кн.: Нейтронная физика. М.: ЦНИИатоминформ, 1988, т.1, с.305.

MULTIDIMENSIONAL ANALYSIS OF CHARGED PARTICLES FROM NEUTRON-INDUCED REACTIONS.

A.A.GOVERDOVSKY

INSTITUTE OF PHYSICS AND POWER ENGINEERING
OBNINSK, RUSSIA, 249020

ABSTRACT. A survey is given of the most recent experimental results obtained using twin gridded ionization chamber constructed at Obninsk, Russia. Peculiarities of (n,α) and (n,f) reactions investigated are discussed. The detailed description of the method of charge particles spectrometry is presented. Selected results on fission fragment characteristics are discussed more in detail. Present experiments and instrumental developments are focussed on correlations between fragment masses, energies and emission angles and on fine structures in fragment parameter distributions.

INTRODUCTION.

The results observed here have been obtained using multidimensional spectrometer based on a gridded ion chamber , where signals from the electrodes are used to derive both the energy of the ionizing particle and the cosine of its emission angle with respect to the normal of the electrodes. The properties of (n,α) and fission reactions can be investigated in detail. This information is very important for a better understanding of the reaction mechanisms . On the other hand the practical applications of the data affect the present and future experimental activity. The main part of information discussed was obtained in the frame work of IAEA Coordinated Research Program (CRP) on evaluation and compilation of Fission Product Yields.

The survey consists of 6 sections:

- Gridded ionization chamber, mechanical setup;
- Generation of signals;
- Spectrometry of alpha-particles; (n,alpha)-reactions;
- Investigation of fission fragments (instrumental topics);
- Experimental mass-energy spectra of fission fragments;
- Measurement of fragment angular distributions.

New trends in our understanding of the fission process including prescission neutron emission, cold and hot fragmentation, dissipation energy are reported.

1.GRIDDED IONIZATION CHAMBER MECHANICAL SETUP

Frish-gridded ionization chamber consists of two parallel plate ion chambers with common cathode, which is 16 cm in diameter. Fig.1 shows the principal scheme of the detector (only one half is presented). The detector is mounted with the plates perpendicular to the neutron beam axis (for neutron-induced fission experiments). The grids consist of wires of 0.1 mm diameter and a spacing of 1.0 mm. The distance between the anode and the grid is 7 mm and between the cathode and grid - 23 mm. This is long enough to stop all the fission fragments with any available energies by the chamber gas just before they reach the grid. The analogous condition can be reached for the α-particles by means of increasing of the gas pressure. The chamber was operated as a flow detector with a 90%Ar + 10%CH_4 for fission experiment and 97%Ar + 3%CO_2 for (n,α)-process investigations. The gas flow was 0.05 l/min, while the gas absolute pressure P was kept at 1.05 10^5 Pa (fission fragments) and 2.30 10^5 Pa (α-particles) with a stability of 0.3%.

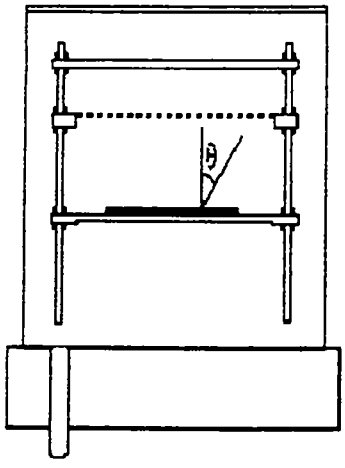

Fig.1.
Scheme of the detector:1- cathode; 2 - grid; 3 - anode; 4 - gas-in-out; 5 - tank; 6 - black area - uranium or other sample.

The detector was mounted in a cylindrical stainless steel tank with the measures: height - 140 mm, diameter - 190 mm, wall thickness - 2 mm.

The samples to be investigated were very thin (<70 $\mu g/cm^2$) layers, prepared from the high-purity materials by vacuum evaporation of UF_4 on a 80 $\mu g/cm^2$ thick Al_2O_3 backing. All targets were mounted in the cathode plane in the center of the chamber (fig.1, black area). The uranium layers were overcoated with 30 $\mu g/cm^2$ of gold to make the cathode conducting. The cathode conductivity is very important since it's necessary to shield the two chambersides from each other with respect to induction by electrical charges moving on one chamberside. But this problem takes place only for the binary decay process like nuclear fission.

2.GENERATION OF SIGNALS

Assume a parallel plate ionization chamber without grid and that all the charged particles enter the detector at the cathode and are stopped before they reach the anode. Let an external power supply (voltage V0) be connected to the anode and the cathode. The free electrons along the ionized track created in the stopping process will then move towards the anode. It is assumed that electron capture in counting medium is negligible and that the amplifier time-constants are long compared to the electron transit time, but very short relative to the positive ions transit time. Therefore we will only discuss electron part of the total ionization current measured in the external circuit of the detector. Neglecting edge effects in the parallel plate chamber this current is [1,2]:

$$I = n(t)\, e\, v / D , \qquad /1/$$

where diffusion current is neglected, and v is the drift velocity of the charged particle, n(t) is the number of the created electrons that is still moving towards the anode at the time t. It is clear that the current is time-dependent, but n(t) is a constant until the first electrons reach the anode. Since the drift velocity of the electrons >1000 times higher than for the positive ions it is seen that until all electrons are picked up at the anode practically all induced charges will be induced by the electrons.

Now, let x be the position of one electron along the ionized track of length S and direction θ relative to the normal of the chamber plates. The total induced charge on the anode by all electrons will be:

$$Q_{ANODE}=Q_A= \int_0^S \rho(x)(1 - x\,COS\theta / D)\, dx , \qquad /2/$$

where $\rho(x)$ is the ionization density along the track. After integration we will obtain the expression used in practice :

$$Q_A = n_0 e\, (1 - \bar{x}/D\, COS\theta), \qquad /3/$$

where

$$\bar{x} = 1/n_0 \int_0^S x\, \rho(x)\, dx \qquad /4/$$

- is the center of gravity of the electron pairs (total number is n_0) along the track. It is obvious that the angular information

can not be available. Let us consider a gridded chamber and assume that the Frisch grid screens the anode ideally from the induction of the moving charges in the space between grid and cathode, and assume that no electrons are picked up on the grid. Then the total charge induced on the anode is $Q_A = n_0 e$. The induced charge on the cathode Q_C will be the same as in the non-gridded case (see eq./3/ , where D is the cathode-grid distance now).

For the single gridded chamber the value of $COS\theta$ associated with any ionizing particle can be found from the two signals forming the quantity:

$$COS\theta = [1 - (Q_C/Q_A)(G_A/G_C)]/(\bar{x}/D) \qquad /5/$$

where G_A/G_C is the gain ratio of the two amplifier chains. It can be determined by converting the detector into a non-gridded ion chamber. The quantity $\bar{x}$ depends on the particle type and energy and can be determined either from calculation using particle stopping powers in the counting medium [3], or experimentally taking into account that the observed distribution of $(1 - Q_C/Q_A)$ value extends from 0 ($COS\theta = 0$) to $\bar{x}/D$ ($COS\theta = 1$).

In eq.5 it was assumed that the anode is completely shielded from the induction of the charges moving between cathode and grid. Actually a fraction σ of the lines of force pass through the grid and end on the anode. Therefore the anode amplitude becomes:

$$Q_A = G_A n_0 e(1 - \sigma\, COS\theta\, \bar{x}/D) \qquad /6/$$

The value of σ is in most designs of the order of a few percent [4]. For our chamber [5] this quantity was found to be 2,6%.

3. SPECTROMETRY OF ALPHA-PARTICLES

3.1. α-PARTICLES OF U-236 SOURCE.

From the COSθ values determined by the above procedure, one can generate the distribution of COS for all particles leaving the sample mounted on the cathode. In the case of angular isotropy, the distribution of COSθ has a rectangular shape. Fig.2 shows an example of the distribution for α-particles, emitted by ^{236}U-source. As can be seen on figure, the angular distribution is distorted for COSθ values closed to 0 ($\theta = 90^0$) due to scattering and self-absorption effects. More detailed information is presented on fig.2. Two dimensional matrix shows , that main part of α-particles backscattered from the

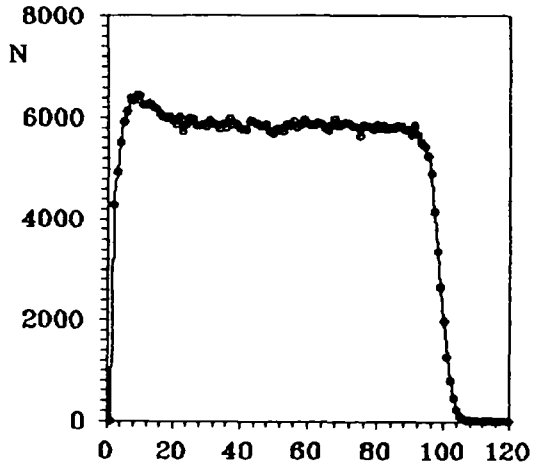

Fig.2. Angular distribution of α-particles emitted by ^{236}U- source with the intensity of 10^3 α/sec.

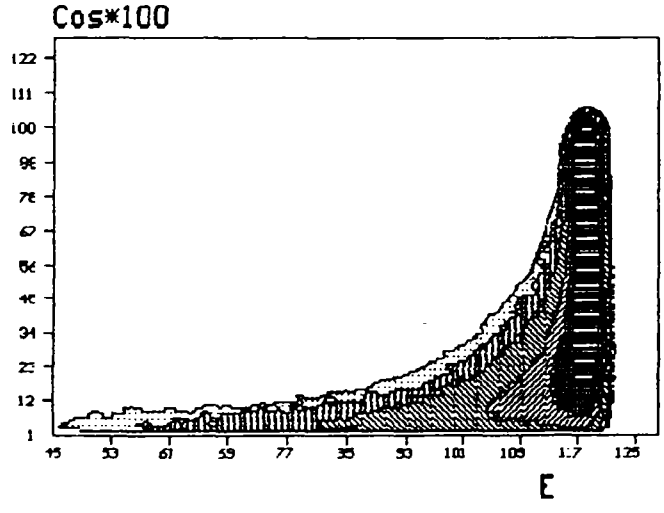

Fig.3. Two-dimensional spectrum cathode-anode (or COSθ-E :energy of the α-particles). Sample thickness was 50 $\mu g/cm^2$. All scattered particles are concentrated in the area of low E- values.

aluminium backing and inside the uranium layer is concentrated in a low-energy region (absolute α-particle yield levels are indicated by different touches). An integration of the distribution will not yield the true sample activity, however for samples with a thickness negligible compared to particle range, the sample activity can be determined from the undistorbed part of the COSθ distribution above a certain COSθ value. In fact, the

simultaneous registration of E and COSθ enables the solid angle, on which the source strength measurement is based, to be chosen such that a relatively high counting efficiency can be obtained in comparison with the conventional low geometry counting.

3.2. SPECTROMETRY OF α-PARTICLES EMITTED FROM (n,α) REACTIONS

In the gas mixture Ar+CH_4 widely used in neutron experiments, hydrogen atoms are present. When the gas is bombarded with neutrons the recoiling protons will ionize and give rise to noise that will reduce the resolution of the detector and increase the background. Therefore, the mixture 97% Ar + 3% CO_2 , for example, should be used as a counting matter in experiments with high-energy neutrons (energy above E_n = 2 - 3 MeV). In this case there are many nuclei which play two important roles : the source of α-particles via (n,α)- reaction, and the counting matter. Detecting mixture contains the isotopes of argon and oxygen with the positive or slightly negative (n,α)-reaction Q-values (reaction heat). All data of the reaction Q-values with the percentage maintenance of isotopes (IPM) are listed in Tab.1.

TABLE 1.

Reaction Q-values and IPM- isotopic maintenance for 97%Ar + 3% CO_2 gas mixture.

ISOTOPE	IPM (%)	Q, MeV
^{36}Ar	0.337	+ 2.002
^{38}Ar	0.063	- 0.222
^{40}Ar	99.60	- 2.486
^{16}O	99.758	- 2.215
^{17}O	0.038	+ 1.819

The energies of α-particles are determined by the incident neutron energy E_n and Q-value : $E_\alpha = E_n + Q - E_r$, where E_r is

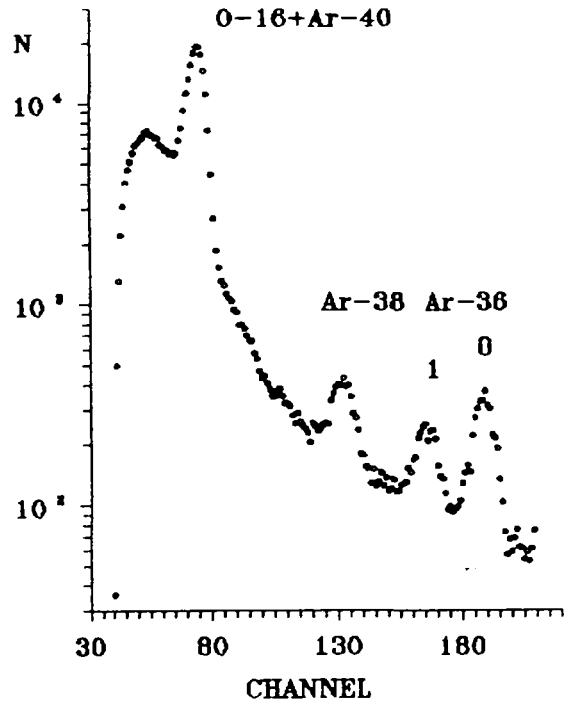

Fig.4.
Anode (energy) spectrum from ion chamber filled by 90%Ar + 3%CO_2 (pressure P = 2.3 Atm) [5]. Incident neutron energy is 5.12 MeV.

the residual nucleus recoil energy. But in fact the total kinetic energy of complementary products $E_\alpha + E_r$ is registrated, if (n,α) reaction is taking place in the gas (argon or oxygen). Fig.4 shows the typical α-spectrum, obtained using gridded ionization chamber irradiated with high-energy neutrons. As can be seen on figure, the spectrum consists of well separated energy lines. Energy resolution is influenced by neutron target thickness (approximately 0.25 MeV in our case) and can be easily improved. The background observed in the spectrum is connected with the (n,p), (n,α)- reactions in electrodes and walls of the detector. The 2.5 MV accelerator (vertical mode) of the Institute of Physics and Power Engineering at Obninsk, Russia, was used to furnish the monoenergetic deuterons (beam was current 20 - 60 μA) for the neutron producing reaction $D(d,n)^3He$ used as neutron source. The thickness of the Ti-D target was 1.4 mg/cm^2; the copper backing was cooled with water.

Fig.5 shows two-dimensional spectrum (cathode-anode) obtained for E_n = 5.12 MeV. One can see two types of separated mono-lines in the data matrix. The first one has low limit on the level of approximately (MAX-cathode signal/2). This effect can be easily understood from eq./5/ above mentioned taking into account that $\bar{x}/D$ value is equal to approximately 0.5 for all α-particles leaving the sample mounted on the cathode. In our case it was the layer of pure ^{58}Ni (thickness was δ = 88 μg/cm^2). The second type of the lines is determined by the (n,α)-reactions in gaseous

medium. In this more complicated case the number n_0 of charged pairs is space-dependent and very strong influenced by the origin and the orientation of the ionized track. Therefore the cathode signal was observed to be very small with the visible probability while the anode one was as maximum as possible. It is the case when the track is originated close to the grid and parallel to it. Of course, the low edge of the gas lines is affected by α-particles angular distribution in the laboratory system, but this influence is disguised very strong. Another problem to be discussed consists in determination of the detection efficiency ε of α-particles moving between the cathode and the grid. It strongly depends on the E_α and the track origin. The value of ε can be calculated with Monte-Carlo method [5].

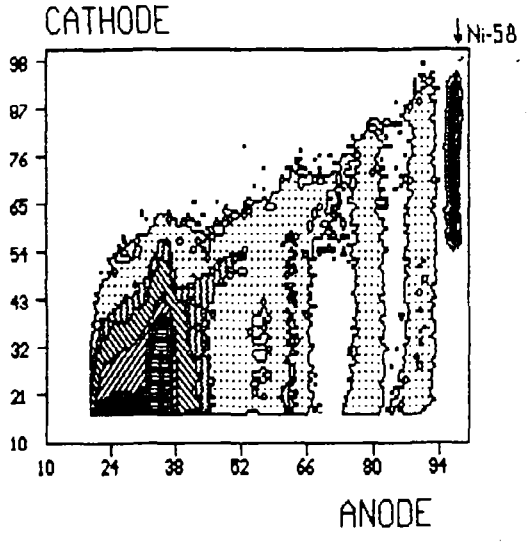

Fig.5. Two-dimensional cathode-anode spectrum (see text).

Fig.6 shows the partial (n,α)

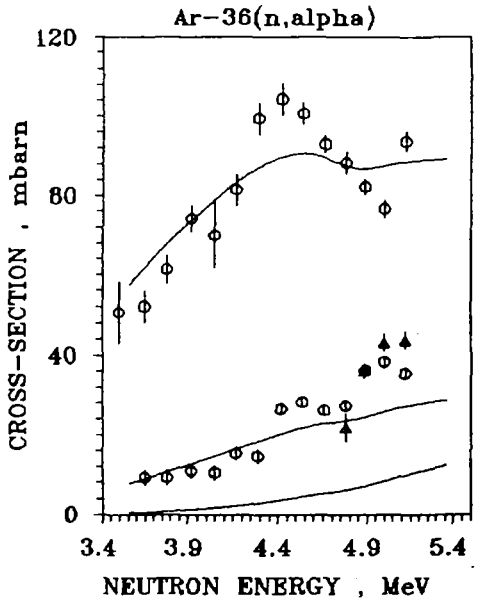

Fig.6. $^{36}Ar(n,\alpha)$ partial cross-sections as a function of the incident neutron energy E_n. Solid curves - are theoretical results [5].

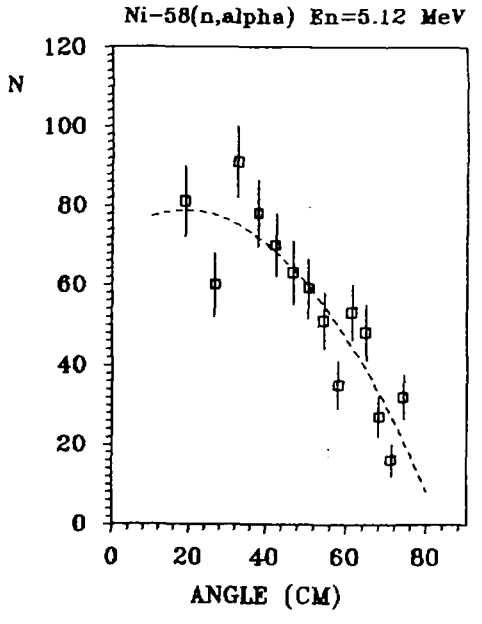

Fig.7.The $^{58}Ni(n,\alpha)$ angular distribution measured with E_n = 5.12 MeV in the center of mass system (CM). Dashed curve - is RMS-fitting.

cross-sections of ^{36}Ar with population of the ground and the first two excited states of the residual nucleus ^{33}S (excitation functions α_0, α_1 and α_2, respectively). Theoretical results presented on fig.6 by solid curves have been calculated in the framework of the statistical model. As can be seen on the figure, contradictions of principle take place between the experiment and the theory.

The (n,α) cross-sections σ_α have been measured relative to the ^{238}U fission cross-section σ_f, which is a strong constant (550 mb) [6] in all neutron energy range from 3 to 5.5 MeV investigated. It was used so-called relative method with geometry "back-to-back", well known in the neutron experiments (e.g. [7]). The uranium target (the thickness was chosen to be 556 $\mu g/cm^2$) was mounted in the cathode plane in the inverse chamberside. Therefore σ_α can be determined from equation:

$$\sigma_\alpha = \sigma_f \, N_\alpha \, n_u \, / (N_f \, n_{ar} \, \varepsilon_\alpha) \qquad /7/$$

where $N_{\alpha,f}$ - are the counting rates of α- particles and fission fragments, respectively; $n_{ar,u}$ - are the numbers of the argon and uranium nuclei irradiated in the neutron flux.

For $^{58}Ni(n,\alpha)$ reaction one energy point was only investigated. The angular distribution of α-particles from the localized source (Ni-foil) is presented in fig.7. It was transformed into the center of mass system ($n^0 + {}^{58}Ni - \alpha + {}^{55}Fe$) [8] :

$$COS\theta^{cm} = [1 - E_\alpha^L \, / \, E_\alpha^{cm} \, (1 - (COS\theta^L)^2)]^{1/2} \qquad /8/$$

$$E_\alpha^{cm} = E_\alpha^L \, (1 + \lambda - 2\lambda^{1/2} \, COS\theta) \qquad /9/$$

and

$$\lambda = (m_n \, m_\alpha \, E_n)/(M^2 \, E_\alpha^L) \qquad /10/$$

where M is the mass of the compound nucleus (^{59}Ni).

As can be seen on fig.7 angular spectrum of α-particles emitted by the excited nucleus ^{59}Ni ($E^* = 14.12$ MeV) was found for transitions to the ground state of ^{55}Fe (α_0 channel) to be anisotropic. On fig.7 N means the number of events. In fact the main part of α's is emitted along the incident neutrons direction. This fact suggested that direct mechanism of α-emission for the α_0-channel of the nickel decay was essential [5]. An integration of α(Ni)-line (or angular distribution) will

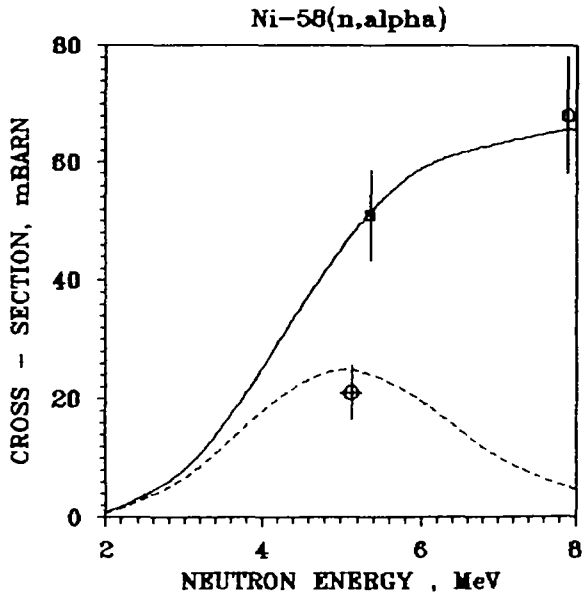

yield the true value of sample activity and after the data evaluation - σ_α - the process cross-section , presented in fig.8. It is necessary to underline that our value of σ_α is only formed by particles moving to the front semisphere of the chamber. A comparison of the experimental and calculated (statistical model [5]) results (see fig.8) suggested that no α-particles were emitted to inverse chamberside of the detector.

Fig.8. ^{58}Ni(n,α)-reaction cross-section: o - present data; and are from [9]. The curves are from calculation : the solid one - total cross-section and dashed one - α0-channel only.

4. INVESTIGATION OF FISSION FRAGMENTS: TECHNICAL ASPECTS.

4.1. KINETIC ENERGY.

The single gridded ionization chamber was discussed above in some detail where the cathode and the anode signals were used to derive the energy and the emission angle θ. In the present case of a twin chamber the common cathode cannot be used, since both fragments induce charge on the cathode and the separation of their influence is impossible. Instead the grid signals are being used.

The grid signals have a more complicated structure than the anode and the cathode signals. Negative charges are induced on the grid as the electrons move toward it and positive charges are induced as the electrons move between the grid and the anode. In practice it is very difficult to operate with the grid signal, since it is asymmetric and bipolar. A much simpler signal is obtained when the sum of the anode and the grid signal is formed. The sum signal is given by :

$$Q_{SUM} = n_0 e \, [1 - (\bar{x}/D) \, COS\theta \,] \qquad /11/$$

In experiment the signals are added by summing them after the charge sensitive preamplifier using wide band amplifiers. The

four signal pulse heights $2P_a + 2P_{SUM}$ contain information about the fission fragment energies $E_{L,H}$ (L,H- mean light and heavy fragment, respectively), masses $m_{L,H}$, angles $COS\theta$, and in the ideal case nuclear charges (for very thin targets only [10]). The pulse height P_a of the amplified anode signal will be proportional to the number of electron-ion pairs n_0 created in the stopping process of the fission fragment. This value is proportional to the fragment energy E_k apart from so-called ionization defect E_d : $E_k = n_0 W + E_d$ (W - is the energy lost per electron-ion pair). The ionization defect is mainly caused by nonionizing collisions between the heavy ions (fission fragments) and the nuclei in the gas. These collisions occur at low projectile velocities and dependent on the detector gas and on the energy, mass and nuclear charge of the projectile being stopped in the gas. Including corrections for grid inefficiency

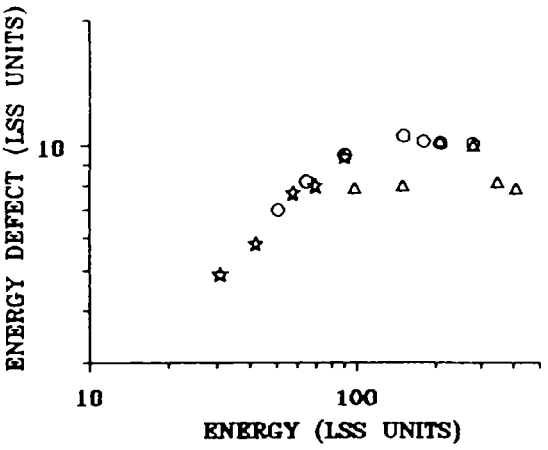

Fig.9. The pulse height defect for the ionization chamber with 90%Ar + 10%CH_4, ref.[15]: solid curve indicates adopted values; different symbols correspond to different heavy ions.

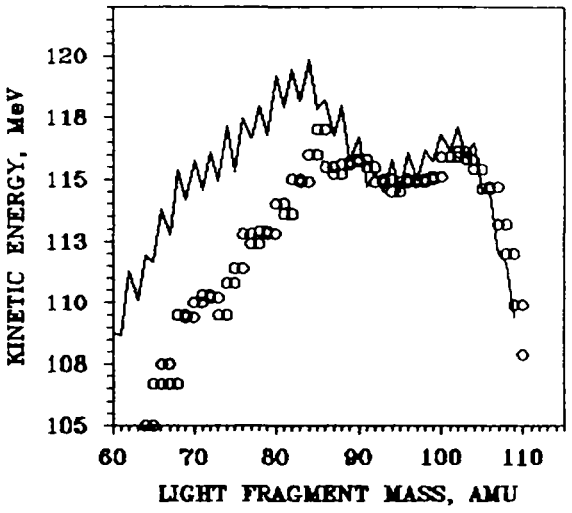

Fig.10. Maximum and observed light fragment kinetic energy for very cold fission of ^{235}U [16].

on P_a the general formula for fission fragment energy will then be :

$$E_k = A_0 P_a + PHD(E_k, Z, m) \qquad /12/$$

where PHD is pulse height defect, it contains mainly E_d; A_0 is the calibration constant for light-mass projectiles (e.g. α-particles), for which the PHD is negligible. A calibration method first proposed in ref.[11] for silicon surface barrier detectors can be adopted for the ionization chamber too [10]. It was

observed theoretically [12] and experimentally [11] that the PHD for different heavy ions can be represented by a single function in the framework of so-called LSS-theory [13-14]. The translation from E_k in MeV to the dimensionless LSS units is:

$$E_{LSS} = E_k \frac{0.8853\ a^0[cm]}{e^2\ [MeV\ cm]} \frac{(Z1^{2/3} + Z2^{2/3})^{-1/2}}{Z_1\ Z_2} \frac{m2}{m1 + m2} \qquad /13/$$

a^0 is the Bohr radius, and $0.8853\ a^0/e^2 = 3.253\ 10^4$ [1/MeV]; indices 1,2 refer to the projectile and to the target respectively; Z,m are corresponding charges and masses. In fact for gas mixture used in fission chamber 90%Ar + 10%CH_4 Z_2 and m_2 are as follows: Z_2 = 16.4 unit charges and m_2 = 36.3 amu.

The PHD for fission chamber similar to the one used here was determined at the tandem accelerator of the Physics Institute, University of Aarhus, Denmark [15]. Typical fragment masses and energies for fragment from fission of ^{235}U were covered. The measured PHDs are plotted in fig.9. The PHD for the light fragments according to eq./12-13/ was found to be from 2.5 to 3.5 MeV, and between 5 and 6 MeV for the heavy fission fragments (of course, these values were adopted at average kinetic energies for all fragments). The reference data practically used are presented on figure by solid curve. For the evaluation of the fission data the PHD_{LSS} versus E_{LSS} values have been tabulated and linear interpolation between the tabulated values has been used only as a function of fragment mass but proton number was also included via relation : $Z = 92\ m_{L,H}\ /236$ (for neutron induced fission of ^{235}U). This is sufficient to find the values needed with the desired accuracy only as a function of $m_{L,H}$.

It can be seen on fig.9, that the discrepancy between experimental data and PHD-correction curve is being taking place for very high E_{LSS}. This energy region is closed to the area of so-called cold compact fragmentation of heavy nuclei. The discrepancy in question affects the mass-energy spectrum as presented in fig.10. As a result the fragment kinetic energies (circles in fig.10) observed experimentally for thermal neutron induced fission of ^{235}U in some cases (yields level is approximately 10^{-6}) are higher than maximum values (solid curve) calculated in terms of fission reaction Q-values using masses tables from ref.[17]. This evidence suggested that the PHD peculiarities around the maximum E_k values should be taken into account more carefully [18].

On the other hand for pure methane used as a working gas it was observed in ref.[19] that the PHD value can be negligible contrary to the results of [20].

4.2.ANGLE DETERMINATION.

The COSθ derivation is based on eq./11/. It is seen that the ratio between the pulse heights P_{SUM}, P_a is given by :

$$P_{SUM} / P_a = 1 - (\bar{x}/D)COS\theta \qquad /14/$$

Taking into account that all fission fragment characteristics are strongly correlated it is sufficient to assume that $\bar{x}/D$ is a function of energy E_k only (see e.g.[10]). Therefore $\bar{x}/D$ can be found experimentally from the P_{SUM} / P_a distribution and eq./14/ can be solved with respect to COSθ. This method allows to determine COSθ with a resolution of 0.034 for separated mass-charge split [10] for spontaneous fission of ^{252}Cf. In our case the analogous value was found to be 0.064 but for all mass-splits around high kinetic energy - more than 110 MeV (U-235). So relatively high FWHM is mainly determined by the thickness of

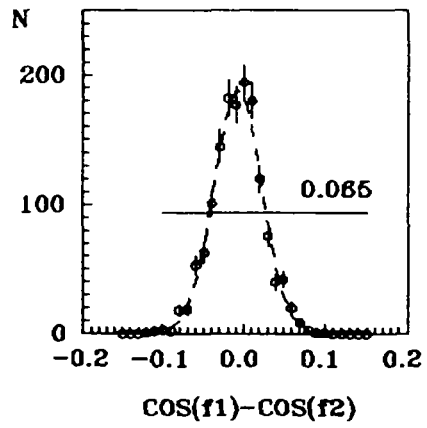

Fig.11. Angular resolution function determined for complementary fragments in thermal neutron induced fission of uranium-235 with the light fragment kinetic energy E_L >110 MeV.

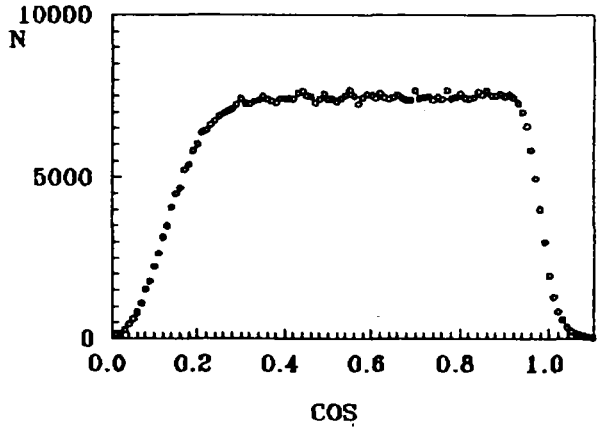

Fig.12. The measured angular distribution averaged over all the fission fragments for U-235(n,f) with E = thermal. The fragments selfabsorption region around COSθ < 0.25 is quite good visible [18].

uranium sample (plus gold and Al_2O_3 backing). Fig.11 shows the COSθ coincidence spectrum for complementary fragments from $^{235}U(n_{th},f)$-reaction. The measured angular distribution averaged over all masses and kinetic energies for the same fissioning system is presented in fig.12. In comparison with the spectrum for α-particles (fig.2) the present one is very strong influenced

by fragment self-absorption effect. This effect is of course largest for small COSθ values and give an important information about the quality of the sample, which can be used in absolute counting rate measurements for neutron-induced reaction cross-sections investigations using the fissile materials for a neutron detection.

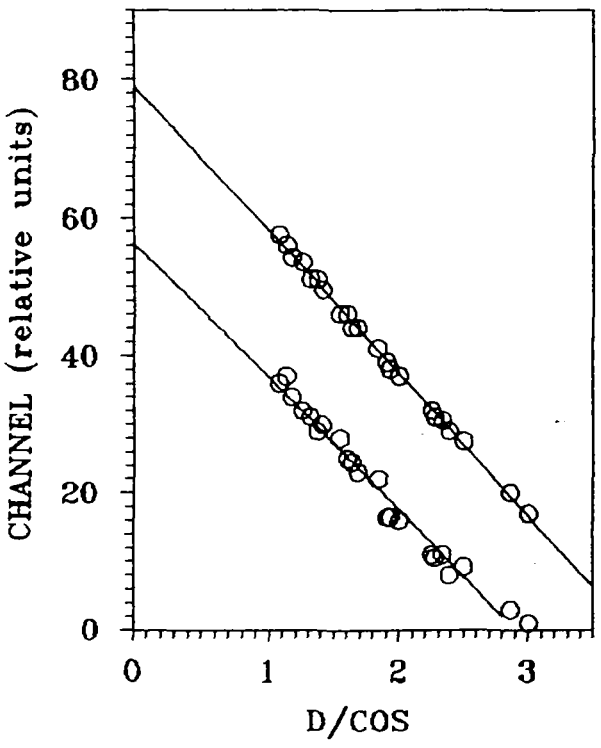

Fig.13. The average energy loss in the uranium target as function of δ/cos The data are measured with 90%Argon + 10% Methane.

The fission fragments loose energy in the uranium sample and the backing. Since the emission angle θ is measured for each fragments it is possible to correct for the energy E_k determined after including the PHD and grid inefficiency corrections. A plot of the average pulse-height spectra as function of δ/COSθ , where δ is a sample thickness, is shown in fig.13 for the light fragment and heavy one separately. On average the loss is of the form constant/COSθ for all fragments in very wide region of E_k. Two lines are shown on the figure used for practical applications. However, it is not possible to determine at which position in the uranium sample a fragment stars. Therefore the correction for the energy loss can only be average correction. This introduces an additional spread in the corrected energy and as a result energy, angular and mass resolutions decrease.

The energy loss in the backing is corrected for rather well since the thickness of backing material that has been penetrated is constant for a given COSθ value for all fission fragments. Some details of the problem are presented in refs.[10,20].

4.3. DETERMINATION OF FRAGMENT MASSES.

In the binary nuclear fission process two fragments - light (L) and heavy (H) - are formed with the primary masses (before

neutron evaporation) m_L^* and m_H^* respectively which are determined with the twin ionization chamber by means of the "double energy method" (2E-method) based on the conservation laws of mass and linear momentum ($m_L^* + m_H^* = 236$ for $^{235}U(n,f)$-reaction).

The fragments mainly get their total kinetic energy in the center of mass system from the mutual coulomb repulsion. The preneutron and postneutron emission energies are given by equations :

$$E_{L,H}^* = 1/2\ m_{L,H}^*\ V_{L,H}^{*\,2} \qquad /15/$$

$$E_{L,H} = 1/2\ m_{L,H}\ V_{L,H}^2 \qquad /16/$$

where $V_{L,H}$ are final velocities and $m_{L,H} = m_{L,H}^* - \nu(m_{L,H}^*)$; ν is average number of prompt neutrons emitted by mass $m_{L,H}^*$. Actually ν-values are determined by the total excitation energy of fragments after the nucleus rupture and full acceleration in coulomb field. Therefore ν depends on the fragment kinetic energy too (see e.g. ref.[21,22]). For thermal neutron induced fission the data [21-25] are used while for fast incident neutrons data of ref.[26] can be adopted. Evaporation of neutrons limits the obtainable mass resolution to approximately 2 units. However, corrections for neutron emission can be avoided for so-called cold fragmentation, where the total kinetic energy TKE $= E_L^* + E_H^*$ nearly exhausts the fission reaction Q-value in which case neutron emission is energetically forbidden.

Neglecting the fragment recoil velocity after neutron evaporation one can obtained the energy (if only 1 neutron is emitted) :

$$E = (m/m^*)\ E^* + (m_n/m)\ E_n - (2E^*/m^*)^{1/2}\ m_n\ V_n\ \cos\vartheta \qquad /17/$$

where index n refer to incident neutron. Since there is no preferred emission direction (angle ϑ) of prompt neutrons, the result for E averaged over several events would give :

$$E_{L,H} = m_{L,H}/m_{L,H}^*\ E_{L,H}^* + \nu(m_{L,H}^*, E_{L,H})\ m_n/m_{L,H}\ E_n \qquad /18/$$

where the second term of the order of 0.3% can be neglected. The result is then :

$$E_{L,H} = E_{L,H}\ m_{L,H}\ /m_{L,H}^* \qquad /19/$$

Conservation of linear momentum gives : $m_L^* E_L^* = m_H^* E_H^*$ and :

$$m_L^* = M_C E_H / [E_L m_L^* m_H / (m_H^* m_L) + E_H] \qquad /20/$$

where M_C is the compound nucleus mass (target + neutron).

The primary mass can be found from eq./20/ with iteration procedure if $\nu(m^*)$-values are known. If the $\nu(m^*)$ data are not known and this is a practically usual situation it is possible to calculate approximate m-values, the so-called provisional masses μ_L and μ_H : $\mu_{L,H} = M_C E_{H,L}/(E_L + E_H)$ which are rather good approximation to the $m^*_{L,H}$ values. The Δm deviation is less than 2 amu for thermal neutron induced fission of ^{235}U [27], but for some physical applications it can be very important [28] :

$$\Delta m_L = \mu_L - m_L^* = M_C (\nu_L/\mu_L - \nu_H/\mu_H) \xi \qquad /21/$$

$$\xi = E_L E_H / [(E_H + E_L)(E_L \mu_L / m_L^* + E_H \mu_H / m_H^*)] \qquad /22/$$

The scale of Δm effect was calculated from eqs./21/ and /22/ to be $0.6(\nu_L - \nu_H)$; Δm changes from positive to negative values. It is clear that for cold compact fission (TKE = Q) experimental mass shift will be zero.

5. EXPERIMENTAL MASS-ENERGY SPECTRA OF FISSION FRAGMENTS.

5.1. THERMAL AND FAST NEUTRON INDUCED FISSION OF ^{235}U.

Experimental fragment mass spectra for several high light fragment kinetic energies are shown in fig.14 for the reaction $^{235}U(n,f)$. The data were separated for emission angles $\theta < 16^0$ relative to the incident thermal neutron direction to eliminate the main part of the correction on the energy losses in the sample. As can be seen on the figure, all mass spectra contain several components grouping near m_L = 102, 96, 90 and 84 amu (nuclear charges according to ref.[29] are Z_L = 40, 38, 36 and 34 respectively). Multidimensional contour map of fission yields $Y-m_L-E_L$ (fig.15) demonstrates this effect in detail. Additional mass components can be observed in the local mass regions $m_L < 84$ amu. Every component is determined by its reaction Q-value and the total kinetic energy, that is why the mass spectra in question are modulated by an individual excitation energy at the scission point E^*. As E_L increases the E^* decreases giving rise

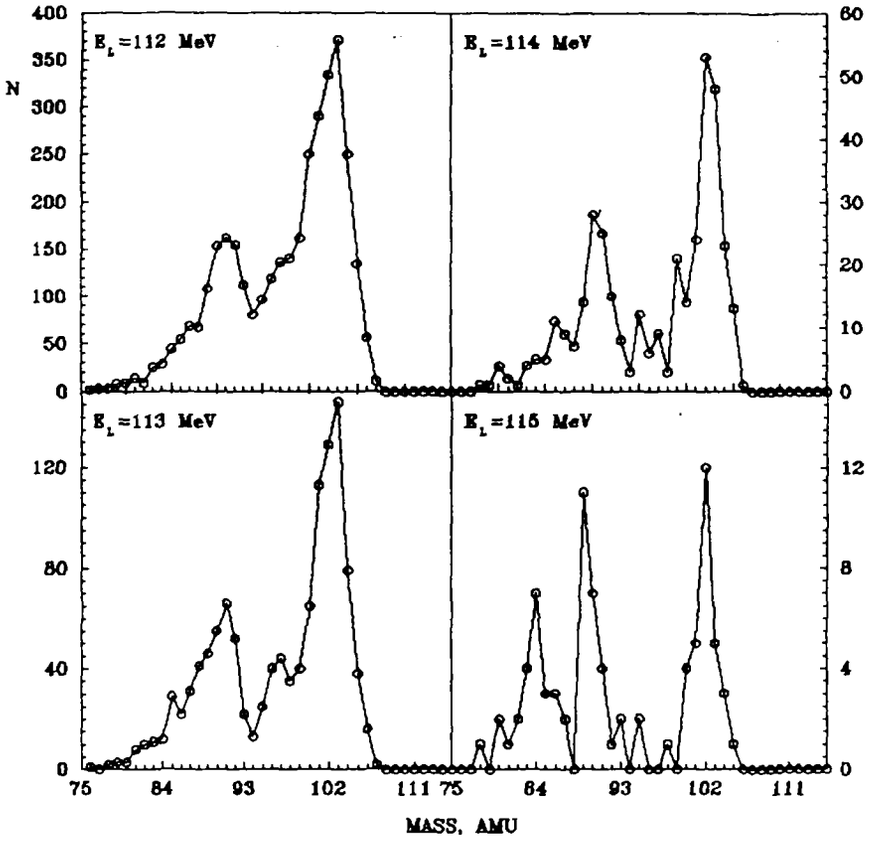

Fig.14. Fission fragments mass spectra for $^{235}U(nth,f)$-reaction.

to cold spectrum changes. So the fraction m_L = 84 amu increases progressively and for E_L = 116 MeV it dominates in the spectrum (fig.15) while the component m_L = 96 amu is negligible already for E_L > 115 MeV. Fig.16 shows the maximum reaction Q-value as a function of light fragment mass (solid line) for thermal neutron induced fission of ^{235}U. The total kinetic energies released in different mass splits (4 mass components mentioned above) with E_L = 114 MeV, for example, are presented in fig.16. No doubt , the component m_L = 84 amu must dominate at very high E_L -values. Quite interesting additional information can be obtained increasing incident neutron energy [16, 18]. A comparison between the thermal and fast (E_n = 1 MeV) neutron

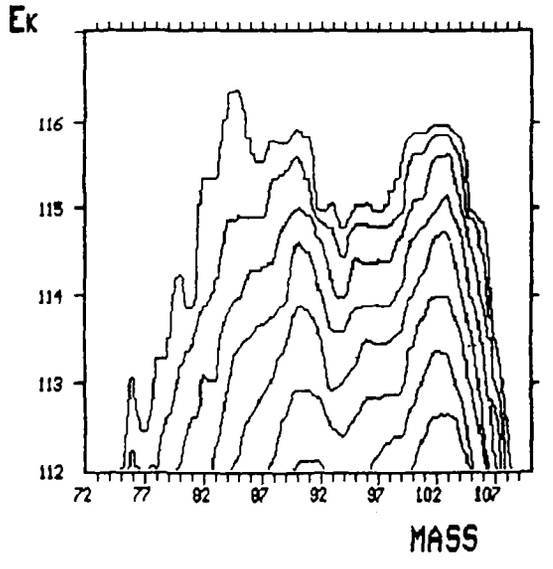

Fig.15. Fragment mass-energy spectrum for thermal neutron induced fission of uranium-235.

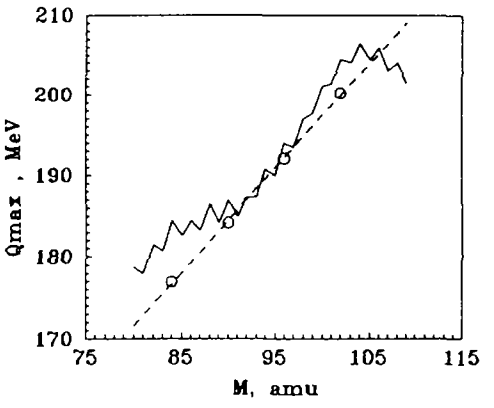

Fig.16. Maximum reaction Q-value as a function of light fragment mass for $^{235}U(n_{th},f)$-reaction calculated using nuclear mass tables from ref.[17]. The circles are the total kinetic energy for several mass-splits at the E_L - window from 113.5 to 114.5 MeV.

induced cold fission spectra is presented in fig.17 for several E_L -values. The data were chosen in the limits of relatively high solid angle $\theta < 40^0$ to increase the statistics. As can be seen on the figure the spectra are similar for both experimental conditions while the reaction Q-values are different : Q(1MeV)=Q(thermal)+1 MeV. For E_L= 116 MeV the mass-component around m_L = 84 amu is pronounced when the incident neutron is thermal. Another situation takes place for E_n = 1 MeV indicating some delay relative to thermal spectra. Fig.18 shows the high energy part of TKE-distribution for both fissioning systems (with the excitation energy at the outer saddle point E_s^* = 1 (E_n = thermal) and 2 MeV (E_n = 1 MeV) [30]). The visible gap between two E_L-

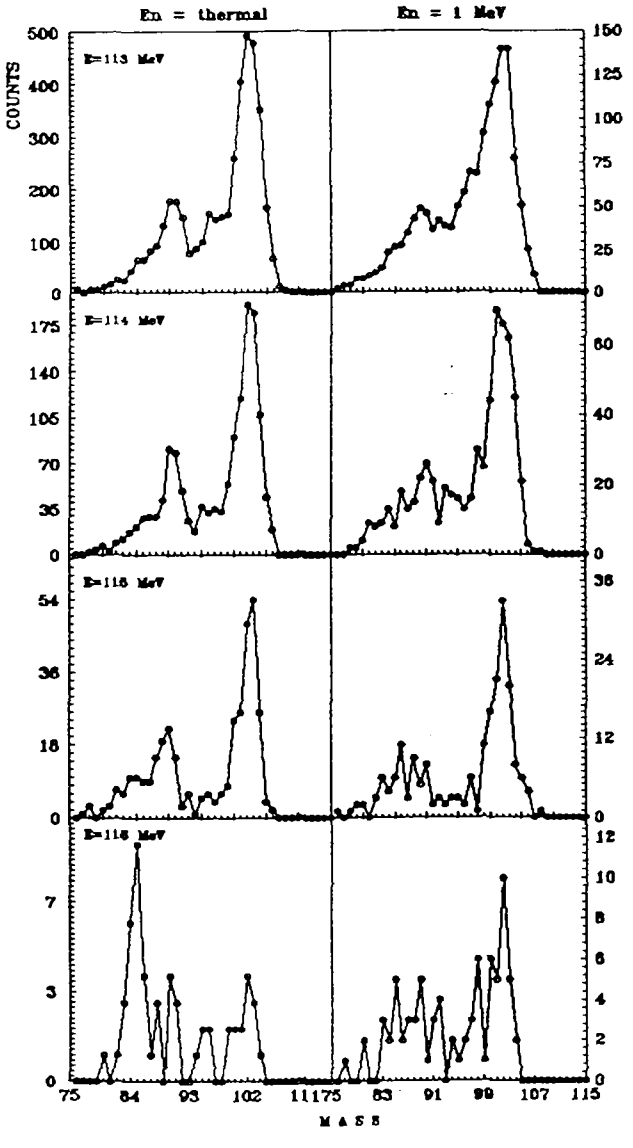

Fig.17. Cold fragmentation mass-spectra measured for two E_n values : thermal and 1 MeV (see text).

curves can be explained as the evidence of E_s^* - conservation during the descent from the barrier top to the scission point.

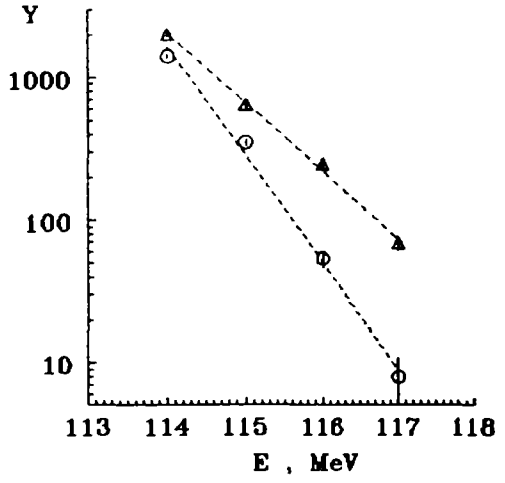

Fig.18. Comparison between the E_L distributions for thermal (0) and fast (Δ) neutron induced fission of U-235 [16],[18].

5.2. COLD FISSION OF ^{236}U

The pile-up of alpha-particles with fission events can increase the background effects (see section 3.2) because the α-activity of ^{236}U-sample is relatively high - approximately 10^3 α/sec. The pulse-height spectrum measured using precision pulse generator connected to the input of the anode preamplifier is shown on fig.19. The solid line represents the Monte-Carlo simulation with real shape of anode signals from α's. On fig.19 area R corresponds to the events of recoiling protons.

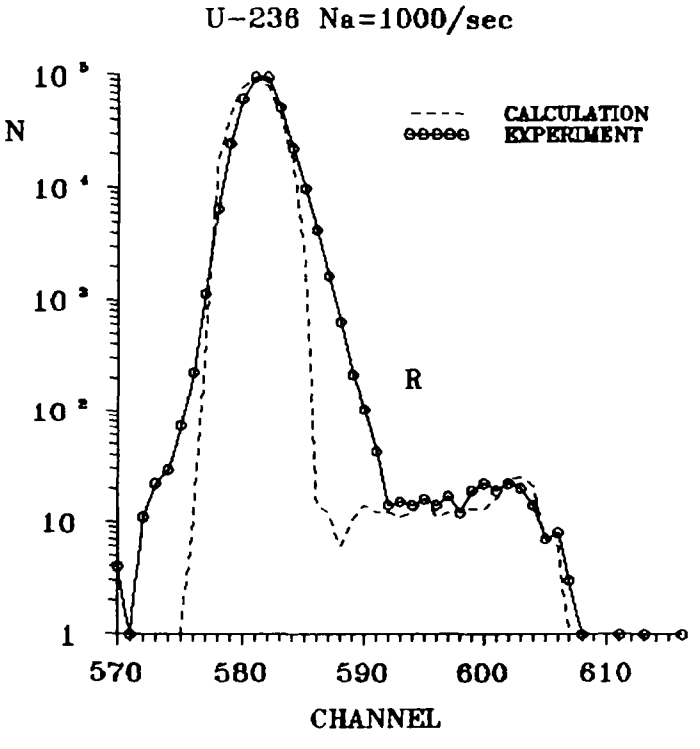

Fig.19. Experimental and calculated (α-f) pile-up spectra for U-236.

The next figure (N20) shows the light fragment mass distributions for fission of ^{236}U with 1-MeV-neutrons. This value of E_n corresponds to the nuclear fission through the outer

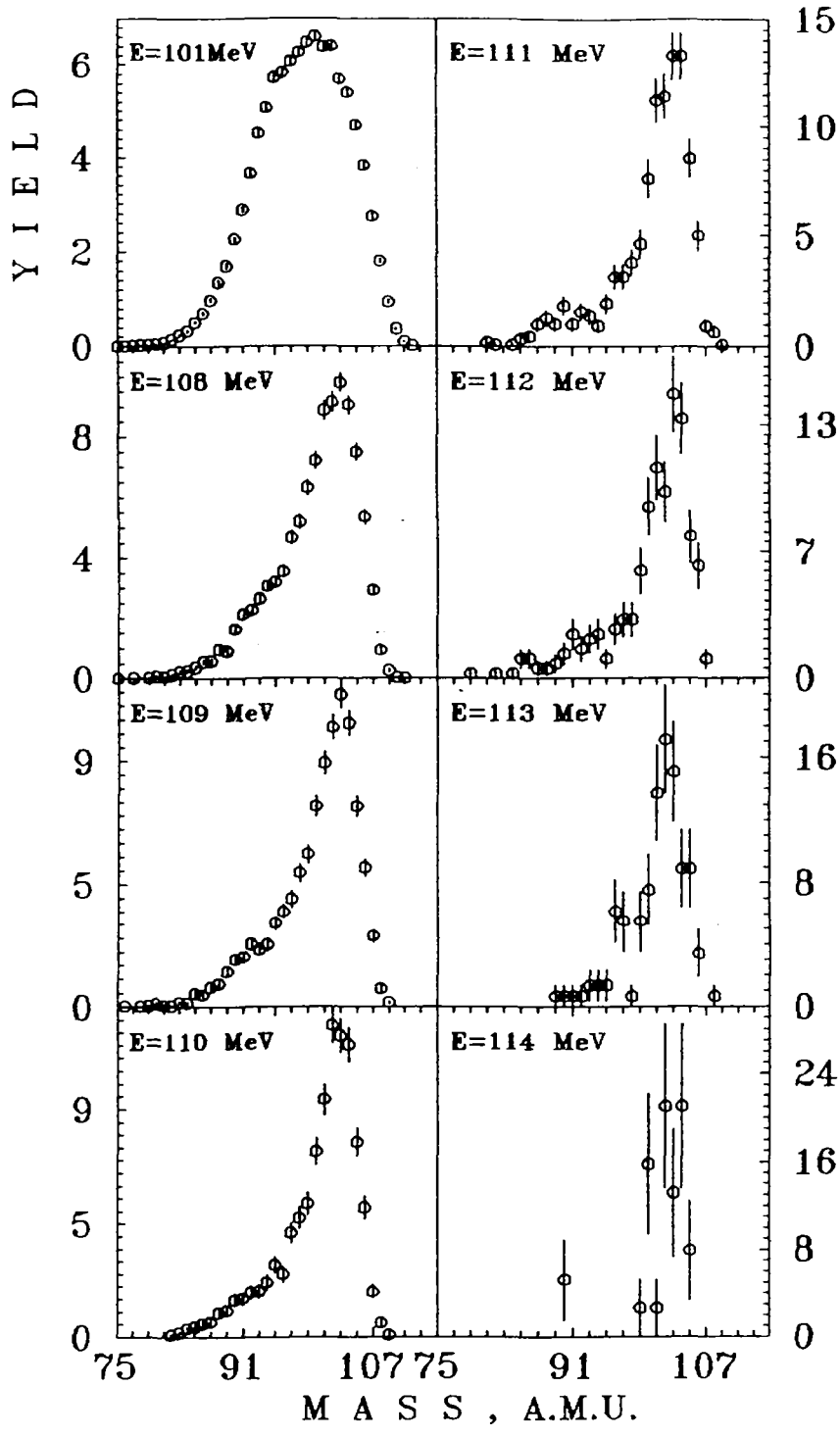

Fig.20. Experimental light fragment mass spectra for fission of uranium-236 with 1-MeV-neutrons ($COS\theta > 0.5$).

saddle point or without the excitation at the barrier top. The comparison with the U-235 data is shown in fig.21. As can be definitely seen all mass spectra are quite different while the excitation energies E^* for all scission configurations are the same due to E_L-separation. This effect can be understood in the framework of quantum-mechanical model of cold fission [31].

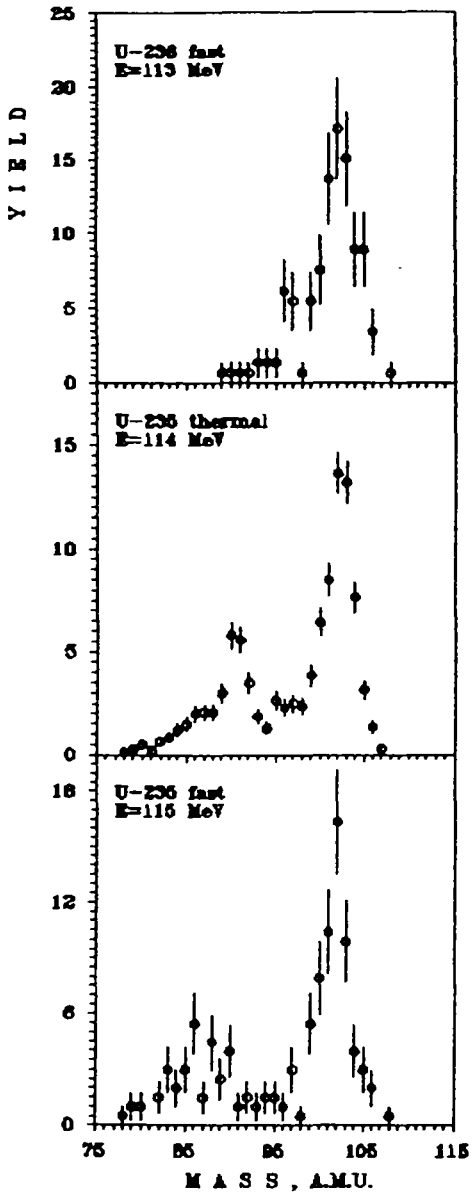

Fig.21. Comparison between cold spectra of uranium-235 (thermal and fast incident neutrons) and uranium-236 for different EL values shifted relative each other by 1 MeV.

In this model the general structure of potential energy surface displays two valleys V1 and V2 separated by a barrier - B_{SCI}. They correspond to nuclear configurations before and after scission, respectively and might be named as a fission value and fusion one. Cold fragmentation is determined by penetrability of the barrier B_{SCI}.

Coming back to experimental data of fig.20 , one first has to realize that the typical development of the mass distributions with decreasing light fragment kinetic energy and therefore with increasing (Q-TKE) really takes place. The energy E_L = 101 MeV corresponds to average value of Coulomb energy realized in nuclear fission of ^{237}U compound-system. Up to about E_L = 108 MeV visible multicomponent structures appear in the spectra an can be fitted by superposition of Gaussian curves. The first moments of the mass components were found to be m_L = 103.1 $\pm$ 0.1, 97.0 $\pm$ 0.2 and 91.1 $\pm$ 0.2 amu (E_L=109 MeV for COSθ>0.5). In comparison with the analogous values for fragments from $^{235}U(n,f)$- reaction [16,18] which were approximately 102, 96 and 90 amu , respectively, the present data (for U-236+n^0) are shifted by 1 amu. This means that one unpairing neutron in ^{237}U is added to the light fragment and all specific properties such as mass-energy correlations of the cold fragmentation as well as nuclear fission on the whole are influenced by nuclear structure of the heavy fragments. The same conclusion can be made from a comparison between the cold mass spectra observed in $^{232}U(n_{th},f)$ [32] and $^{233}U(n_{th},f)$ [29] reactions.

On the other hand, at least one well pronounced mass component around m_H = 134 amu plus complementary part (102 and 103 amu for ^{235}U and ^{236}U , respectively) must be strongly affected by shell effects and can be unaffected by nucleon composition of fissioning system. Fig.22 shows an example of mass-distribution fitting with superposition of Gaussian curves for two compound nuclei. In fig.23 one can see free-energy dependencies of mass dispersions associated with $134/(M_c-134)$- components of cold mass- spectra for U-235 and U-236 - fission . The free energy in

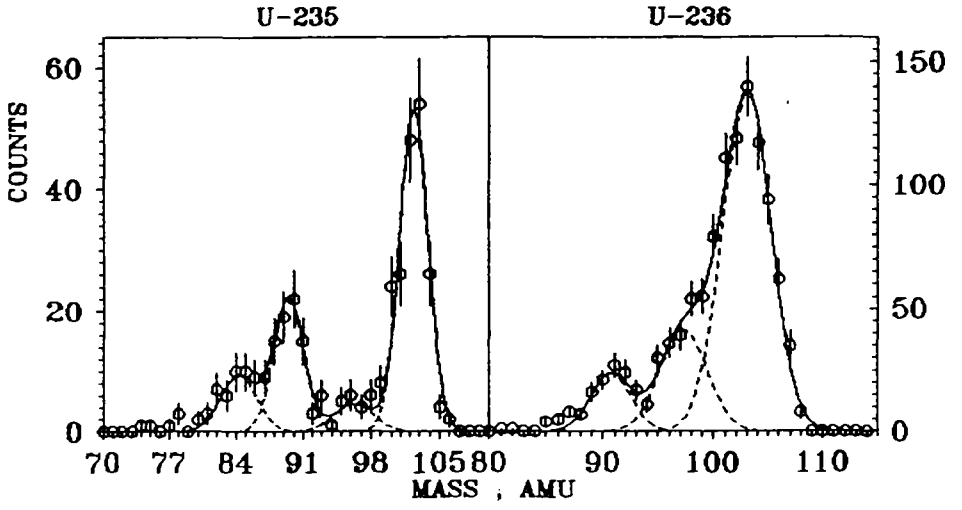

Fig.22. Fitting of cold mass-spectra for fission of U-235 and U-236 . Experimental data are evaluated for solid angle $COS\theta > 0.75$ in both cases.

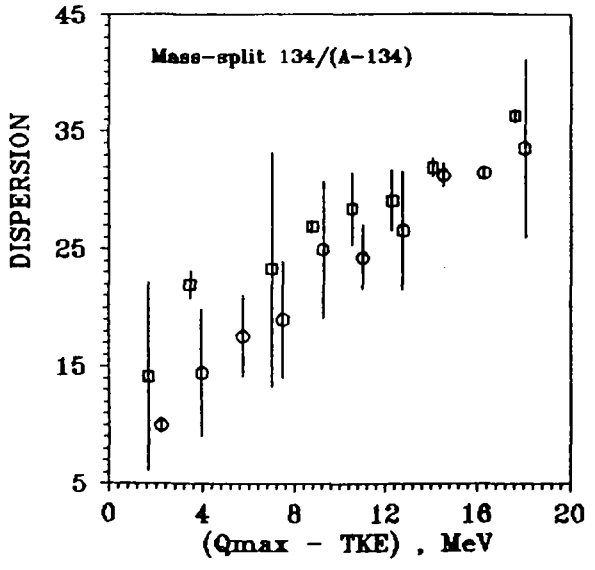

Fig.23. Mass-dispersions of the spectrum component around heavy fragment mass m_H = 134 amu for fission of uranium-235 (O) and -236 ( ) as functions of excitation energy at the scission point.

our case is the difference $E_F = Q_{MAX}$ - TKE , where Q_{MAX} is a maximum Q-value of fission reaction determined according to next relation :

$$Q_{MAX} = MAX [M(^{235,236}U+n^0) + E_n + B_n - E_R - m_L - m_H] \quad /23/.$$

In /23/ B_n is the neutron binding energy in (uranium-target + neutron with the energy E_n)- compound system [33]; E_R is recoil energy after neutron capture .

Fig.23 shows the identical behaviour of σ_m^2 -values for both fissioning nuclei with E_F . Having in mind that free energy can be completely exhausted by excitation one for cold fragmentation fractions the fission valleys associated with 134 + complementary mass splits of $^{235,236}U$ are assumed to be identical . For quasiequilibrium statistical formation of mass distributions the dispersion is described by single relation : $\sigma_m^2 = T / C_m$ (see e.g. ref.[34]) for $T >> \hbar\omega$, where T is the nuclear temperature defined as $T = (E^*/a)^{1/2}$ and a is so-called level density parameter [35] in the corresponding point of potential energy surface ; C_m is the stiffness coefficient for mass-asymmetric distortions ; $\hbar\omega$ - is the effective frequency of oscillations for these distortions. As can be seen on fig.23 the general characteristics C_m of fission valleys are similar for both fissioning nuclei : ^{236}U and ^{237}U . Analogous conclusion can be made for another fission valleys. At the same time the kinetic energy distributions (mass integrated) presented in fig.24 for two fissioning systems display the coincidence with one another. Coming back to fig.21 one ought to assume that the scission

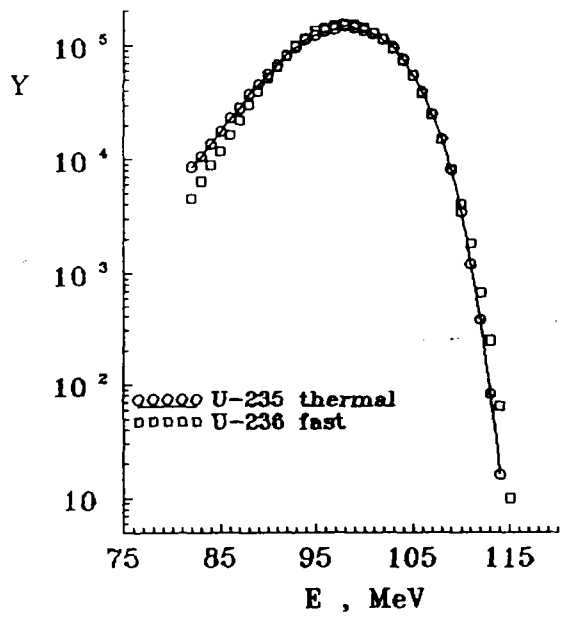

Fig.24. Mass-integrated distributions of light fragment kinetic energy for thermal neutron - induced fission of U-235 and fission of U-236 with 1 MeV-neutrons. Data for U-236 are normalized to U-235-statistics.

barriers B_{SCI} play an important role in nuclear cold fragmentation process because integral population of each mass or fission valleys was demonstrated above (fig.22 -24) to be very strong influenced by corresponding saddle points just before the nuclear passage to scission.

5.3. OBSERVATION OF PRESCISSION NEUTRONS IN FISSION OF URANIUM.

It was mentioned in section 4.3 (eq.21 and 22) that the provisional $\mu_{L,H}$ masses observed experimentally are being slightly shifted in respect to primary masses $m_{L,H}$. This shift is affected by difference $(\nu_L - \nu_H)$ between numbers of prompt neutrons emitted from the light and the heavy fission fragments . However, the possible neutron emission from the compound nucleus

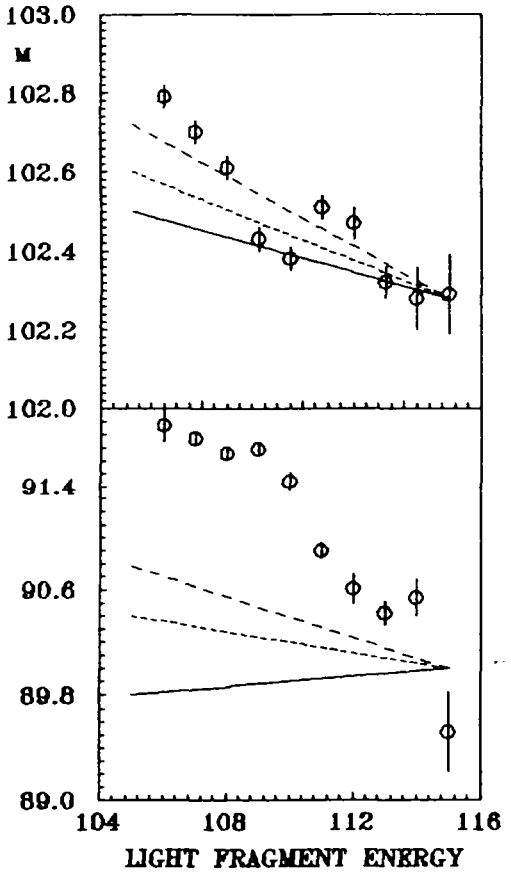

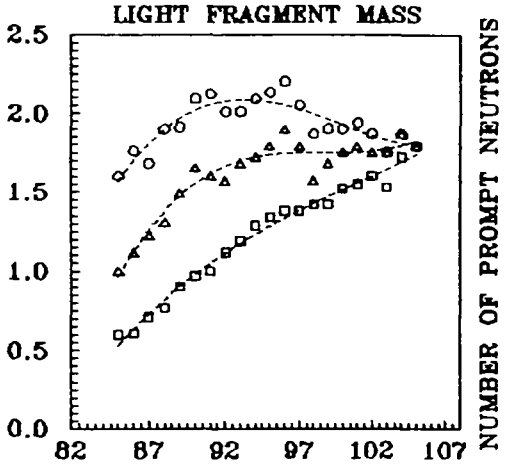

Fig.26. ν_L data as a function of light fragment mass : - [23], - [24] and - [25].

Fig.25. Experimentally observed values Δm_L for two pronounced mass components around m_L = 102 and 90 amu (U-235 + thermal neutron). Lines are the theoretical predictions based on the $(\nu_L - \nu_H)$-data averaged over TKE and presented in fig.26 : dashed - [25], shot dashed - [24] and solid line - [23].

at the stage of motion between the saddle point and scission one must be taken into account . In this case the shift discussed above is $\Delta m'_L = \nu_{PRE}\, m_L / M_C$. Its sign is essentially positive. Experimentally observed values of Δm_L can be seen on fig.25 in comparison with predicted values calculated assuming that the total amount of prompt neutrons are emitted from the fragments after acceleration in mutual Coulomb field (average data are

presented in fig.26) . This hypothesis is approximately correct for mass valley m_L = 102 amu . However, an additional part of neutrons is needed for explanation of relatively high mass shift Δm_L of the component around the m_L = 90 amu. This part was assumed [28] to be associated with **prescission neutrons** emitted during initial stage of the descent from saddle to scission. Of course , the partial contribution of prescission neutrons ν_{PRE} is very small relative to $\bar{\nu}_p$ (10^{-3}) therefore it can be neglected in practical applications. But the physical aspects are very interesting because the neutron emission from unrupted nucleus after saddle configuration needs a much time for the descent and may be influenced by nuclear viscosity effects in low-excited and high-deformed fissioning system. Therefore it is possible to deduce the fission or prescission time τ_{PRE} as the time difference from the moment when the system has obtained enough excitation energy to start to evaporate neutrons . The prescission multiplicities observed for example in fusion-fission reactions with heavy ions were used to determine τ_{PRE} values which were found to be in the order of a few 10^{-20} sec [36-40].

Neutron-fragment angular correlations in $^{235}U(n_{th},f)$ as a function of neutron energy and fragment mass are presented in [41]. The prescission neutrons component was observed to be in quite good agreement with our conclusions (see e.g. figs. 1,2,3 and 4 in ref.[41]). In addition the energy of those neutrons was measured to be less than 0.5 MeV (approximately).

Since the total kinetic energy is anticorrelated with the excitation energy of the fragments, measurement of the correlation of ν_{PRE} with TKE may throw much light on the emission mechanism. It was observed in [42,43] that the angular anisotropy averaged over all fragment masses initially increases and then saturates at higher TKE . From the comparison of the calculated and experimental anisotropies the fraction of prescission neutrons as a function of TKE could be deduced for an assumed neutron emission spectrum. Analogous situation have been analyzed in ref.[44] for the spontaneous fission of ^{252}Cf. The careful analysis of average prompt neutrons spectrum is presented in [45].

Increasing of incident neutron energy leads to the rapid growth of prescission neutrons emission. So in ref.[46] the ν_{PRE} - value was found to be approximately 0.1 in comparison with ν_p for E_n = 14.7 MeV.

5.4. HOT FISSION OF ^{236}U (COLD DEFORMED FRAGMENTATION).

It was mentioned above that at high kinetic energies of the fragments the mass distributions exhibit marked fine structures . They fade away for average E_k , then surprisingly come back at very low kinetic energies for fission of ^{245}Cm with thermal neutrons [47-49] and $^{232,235}U$, ^{239}Pu [32]. For $^{236}U(n,f)$ reaction this effect have been observed too. Fig.27 shows the contour map of fission yields at very low light fragment kinetic energies , i.e., well below average values. One first has to realize that the fine structures in mass spectrum do exist therefore the excitation energy of fissioning system must be very low. At the same time the well pronounced slope of figure as a whole is visible due to prompt neutrons evaporation from fission fragments. It is clear that the difference (Q - TKE) is exhausted by deformation energy of fragments. For cold nuclei proton pairing is effective and in experiment the pairing shows up as a strong odd-even effect in the charge yields. This problem was discussed in ref.[32] in detail. Marked o-e effects were uncovered which, similar to the mass distributions , are conspicuous at large TKE and fade away as a energy approaches average values. One may speak of cold **COMPACT** and cold **DEFORMED** fission as two limiting possibilities of the fission process.

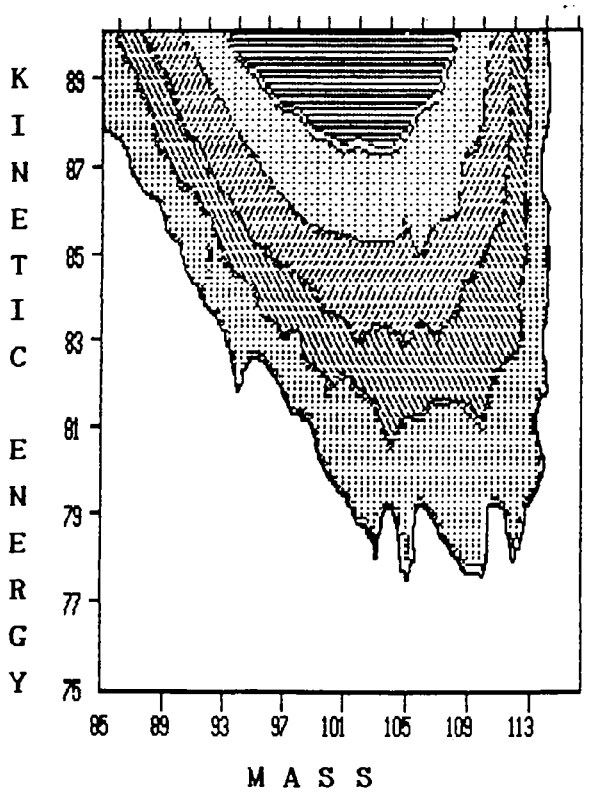

Fig.27. Mass-kinetic energy contour map for fission of ^{237}U in (n,f) reaction. Provisional μ-masses only presented here because the neutron emission is quite intensive and can not be included into data evaluation. Figure demonstrates the neutron-sensitivity of twin ion chamber.

5.5. HIGH-ENERGY NEUTRON INDUCED COLD FISSION.

Excitation energy at the saddle point of fissioning system is determined by incident neutron energy and can be distributed between prescission kinetic energy E_k^{PRE} (minor fraction of TKE)

and internal excitation ε (see section 5.1, fig.18). The latter affects the fragment mass- spectra at high values of TKE while

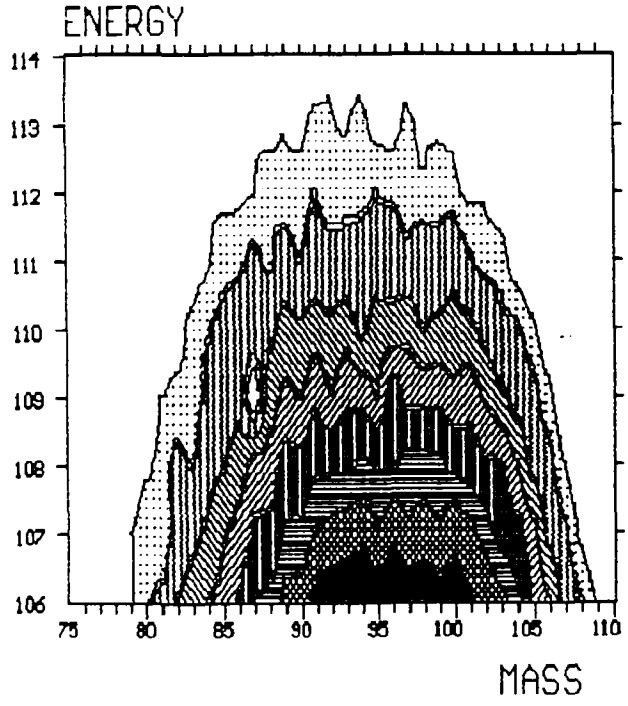

Fig.28.
Fission fragment mass-energy correlations observed for U-235(n,f) reaction . Neutrons with energy from 3 to 7 MeV were obtained using Be(d,n)- reaction as a neutron source (thick target). Total counting statistics was 5 millions.

the growth of prescission energy E_k^{PRE} expands the region of E_L in which the mass-spectra can be observed. Experimental yield- mass-energy contour map measured for fission of ^{235}U induced by high energy neutrons (average value of E_n was approximately 4.5 MeV) is plotted on fig.28. One can see on the figure the conservation of fine structure for all kinetic energies from 106 MeV up to 114 MeV. This is a consequence of an overlap of mass spectra associated with different incident neutron energies of primary flux. In addition the processes of prescission neutrons evaporation effectively modulate the contour map. On the other hand , small admixture of fissions above the (n,n'f)- threshold complicates the picture in question.

6. MEASUREMENT OF FRAGMENT ANGULAR DISTRIBUTIONS.

The angular distributions can give basic information about the fission process. One of the useful concepts in nuclear fission phenomena is that of the transition nucleus [50]. It was suggested that low-energy fission may be understood in terms of one or a few levels in the transition nucleus because most of the excitation energy goes into deformation energy during the passage from initially excited system at ground state deformation to the more deformed saddle configurations. Each one of the transition

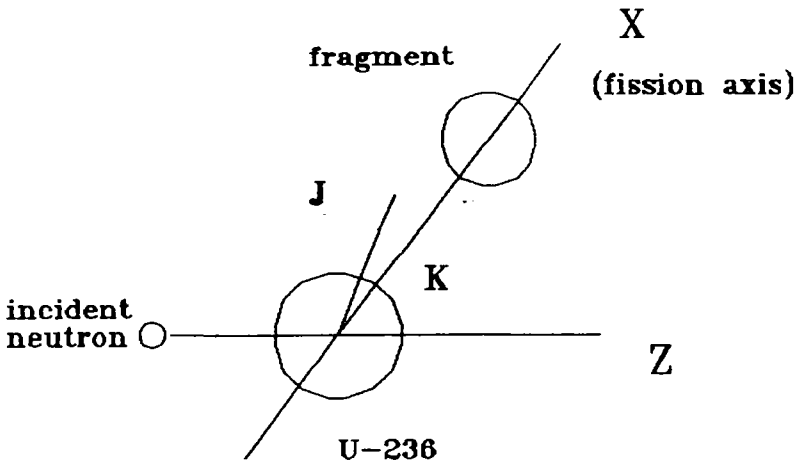

Fig.29. Angular momentum coupling scheme for a deformed heavy nucleus . The vector J defines the total angular momentum. The space-fixed axis was defined as the incident neutron beam direction.

levels are described in terms of the quantum numbers, J, K, M, π, where J represents the TOTAL angular momentum, π is the parity of the level, K is the projection of J on the nuclear-symmetry axis, and M is the projection of J on a space-fixed axis (neutron beam axis). The relationship between them is shown in fig.29.

If one assumes that K is a good quantum number in the passage of a nucleus from its transition state at the saddle point to the configuration of separated fragments (scission point), the directional dependence of the fission fragments is uniquely determined (fission fragments separate along the nuclear symmetry axis). For fast neutron induced fission of even-even target nucleus ^{236}U with zero spin, value M is $M = \pm 1/2$ and the fission fragment angular distribution is give by [51],

$$W^{J}_{-^{+}1/2,^{\pm}K}(\theta) = (2J + 1/4)\,[\,|d^{J}_{+1/2,K}(\theta)|^{2} + |d^{J}_{-1/2,K}(\theta)|^{2}\,] \qquad /24/,$$

where the D-functions $d^{J}_{M,K}(\theta)$ are defined in refs.[52,53].

Eq./24/ is normalized so that :

$$\int_{0}^{\pi} W^{J}_{^{\pm}1/2,^{\pm}K}(\theta)\,\sin(\theta)\,d\theta = 1 \qquad /25/.$$

It is interesting that different deformations at the saddle point allow for different sets of J, K, π values [54]. This problem is discussed in detail in ref.[55].

The angular distributions have been investigated in several previous measurements, refs. [20, 56 - 58] (for $^{235}U(n,f)$) and

[51, 59, 60] (for ^{236}(n,f)). The measurements are mostly made as averages over all masses and kinetic energies of the fragments.

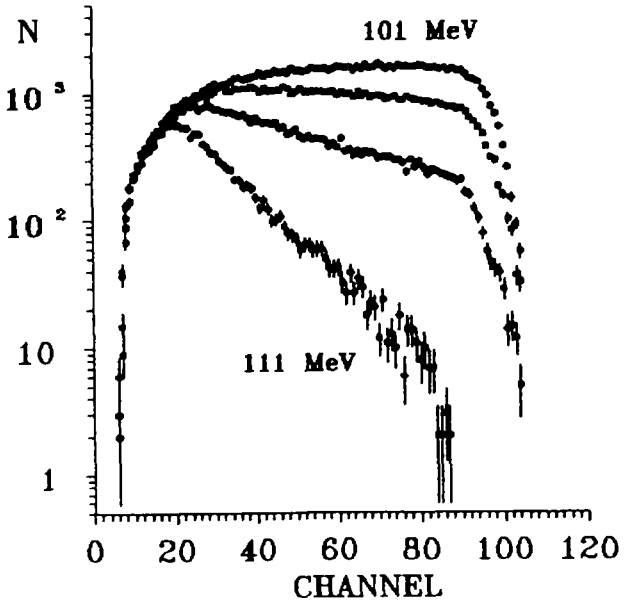

Fig.30. Experimental angular spectra plotted for E_L from 101 MeV to 111 MeV (U-236nf).

Here we wish to demonstrate the results of multidimensional measurements of the fission fragment angular distribution for the ^{236}U(n,f) reaction in correlations with the mass and the kinetic energy distributions covered all region of scission configurations between the cold fragmentation (scission near the saddle point) and usually observed fission process which can be characterized by fragment separation beyond the saddle point.

Fig.30 shows the primary experimental Y(COSθ) spectra measured for ^{236}U fission induced by 1-MeV-neutrons at different light fragment kinetic energies : from 101 MeV (approximately average value for U-236 fission) to 111 MeV. In fig.30 channel is 100 COS and N is counting statistics. The data presented there are averaged over all fragment masses. A drop in yields is seen for small COS θ values. This is mainly caused by absorption in the target and backing (see section 4.2). Therefore the data were only transformed into angular distributions for $5^0 < \theta < 65^0$. Final results are presented in fig.31. As can be seen on the figure the fragment angular distributions change essentially with kinetic energy. This evidence suggested that the stage between saddle point and the scission one plays an important role in angular distribution formation affecting the K-spectrum . The angular distributions for different mass components associated with mass-channels discussed in sec.5.1-5.2 are quite similar to the mass-averaged ones. Since respective statistics is relatively low one may only analyze the fragment anisotropy R of Y(θ) determined as R = Y(COSθ = 0.45)/Y(COSθ = 0.85) for different mass splits as a function of light fragment kinetic energy E_L.

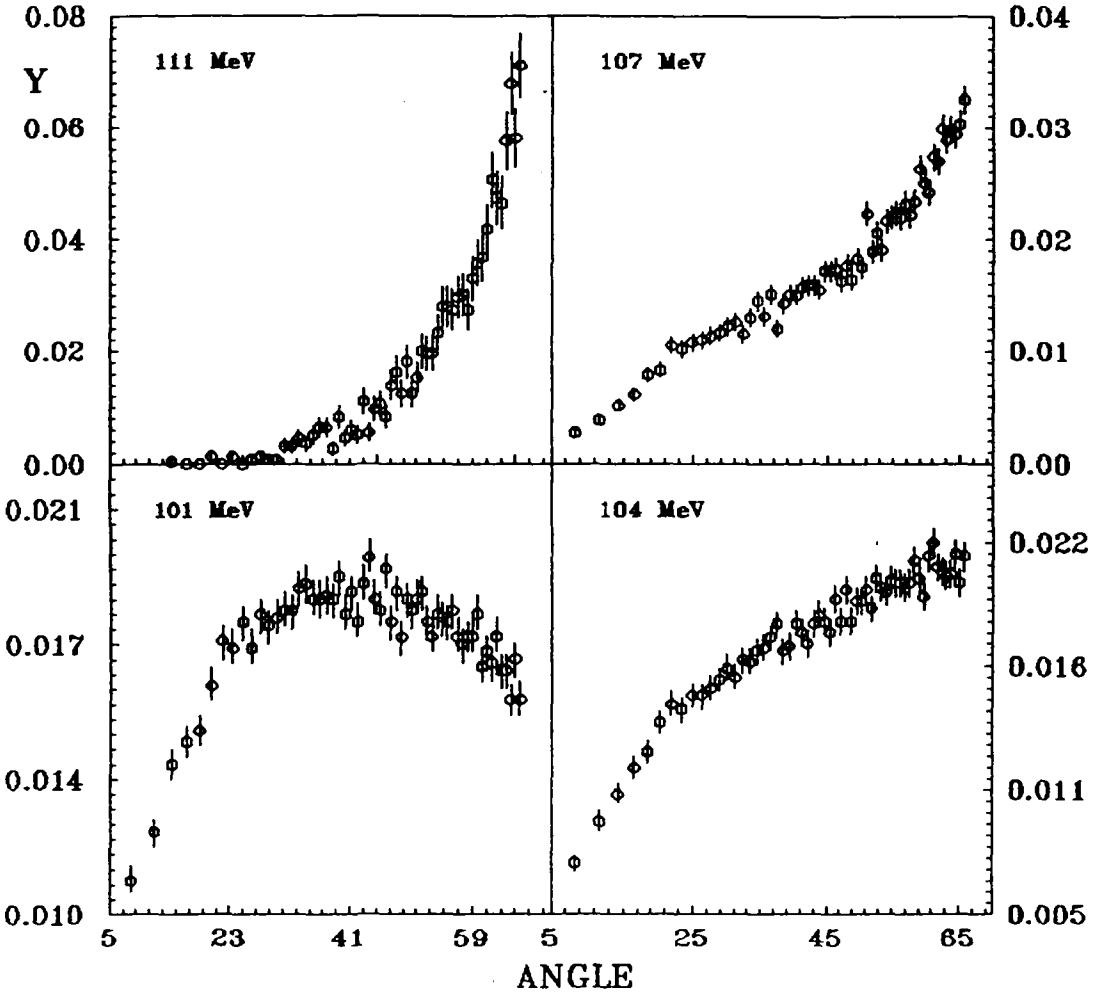

Fig.31. Fission-fragment angular distributions associated with different stages of the passage of nucleus from its transition state to the configuration of separated fragments.

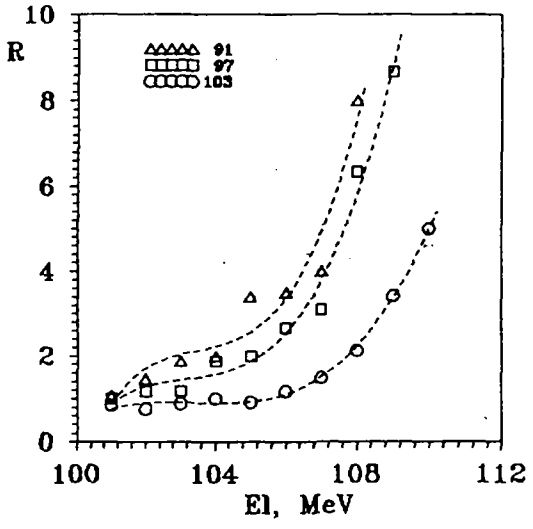

Fig.32. Fragment anisotropies R determined for separated mass valleys of U-237 compound nucleus. Dashed curves are fittings with legendre polynomials. EL is light fragment kinetic energy.

These data are presented in fig.32. One can see that rapid transformation of angular spectra appears at very high total kinetic energies associated with scission configurations of relatively cold nuclear rupture. In addition this effect magnitude depends on the fission valley or mass-channel.

No doubt , for the valley determined by strong shell effects (double-magic heavy fragment with m_H = 134 amu plus complementary light fragment) the transformation of $Y(\theta)$ is relatively small in comparison with another valleys. Coming back to fig.25 one ought to assume that two essentially different processes such as prescission neutron evaporation and $Y(\theta)$- change are caused by the same reason - nuclear viscosity in low-excited deformed compound system after fission barrier penetration. This problem is mostly investigated theoretically in the framework of liquid drop model [61-64] for hot fissioning systems. The diffusion model was applied to the analysis of nuclear fission and discussed in review [65]. In considering this point for low-energy fission we must refer to work [66]. The dissipation energy E_{DIS} caused by intensive exchange between internal degrees of freedom and collective ones due to viscosity effects was determined from fragment charge odd-even peculiarities to be approximately 5 - 6 MeV for uranium-236. It only was the average level of E_{DIS}. Careful analysis of fission fragment

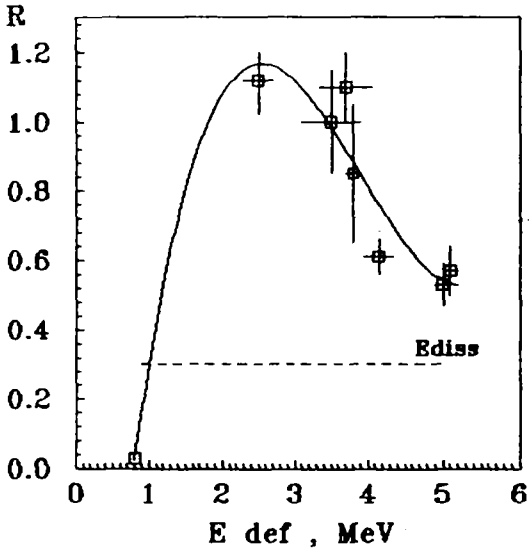

Fig.33.
Behaviour of dissipation energy with nuclear elongation. Experimental (evaluated) points are from [67]. The dashed curve is average level of dissipation energy [66].

mass-dispersions [34,67] allowed to determine the heating of fissioning nucleus (in units of E_{DIS}) as a function of ΔE_{DEF} :

$$R = E_{DIS} / \Delta E_{DEF} = f(\Delta E_{DEF}) \qquad /26/$$

where ΔE_{DEF} is the difference between deformation energies at the saddle point and the scission one. This function is presented in fig.33. As can be seen on the figure the initial stage of the nuclear passage from saddle point may be characterized by biggest viscosity for $\Delta E_{DEF} > 1$ MeV. This conclusion is confirmed theoretically in the quantum-mechanical model [68,69]. Comparing

the data of figs.25,32 and 33 one can assume that all three effects (ν_{PRE} , $Y(\theta)$, E_{DIS}) discussed here are very closely connected with each other.

As to fragment angular distributions the projection K of total angular momentum J is affected by viscosity effects and can not be good quantum number. At the same time there are two another explanations of angular feature. . The first one is connected with the scission barrier penetration at the scission point. This barrier has the definite transition states spectrum influenced by deformation of fissioning nucleus. It is possible that the selection of (J,K,π)- combinations plays a preferable role in angular distribution formation. In that case it is possible to study so exotic object like scission barrier. The second hypothesis is based on well-known strange fact that fragment kinetic energy decreases in fission through vibrational resonances [34,70,71] . An admixture of vibrational mode to fission probability can affect the angular spectra at the initial stage of the descent.

CONCLUSIONS AND PROSPECTS.

Charged particle spectrometers based on twin gridded ionization chamber open a wide field of research in low energy neutron-induced reactions such as (n,α) and (n,f). Fission fragment parameters, like mass, kinetic energy and emission angle can now be measured with high accuracy near the fission thresholds. Dedicated detector system with fast multiparameter data acquisition system allow the measurement of correlated fragment parameters.

The presented results show the importance of shell effects and neutron emission processes for understanding of nuclear fission. In experiment the two limiting scission configurations may be distinguished by the kinetic energy release observed. The Coulomb repulsion between the fragments will lead to high TKE for a compact scission configurations, while low kinetic energies correspond to strongly deformed configurations. So-called hot fission is followed by neutron emission from accelerated fragments. On the other hand a number of neutrons are emitted just before nuclear rupture . Primary observation of prescission neutrons should be done using ion chamber with neutron registration channel.

The presented fission fragment angular distributions show very interesting role of initial stage of nuclear shape evolution after saddle point penetration. Future experiments can be performed to study the fission through vibrational resonances associated with the states of intermediate well of fission barrier. Resolved resonances region is very important too having in mind that pure (J,K,π)-sets can be included into investigations.

Practical applications of ionization method are very wide. There are sample and backing investigations, determination of absolute α-activity of targets, measurements of neutron-induced reaction cross-sections, neutron dosimetry.

ACKNOWLEDGEMENTS.

The author have to thank Prof.A.Ignatyuk, Prof.F.Gonnenwein, Prof.J.P.Theobald, Prof.V.Pashkevich, Dr.F.-J.Hambsh, and Dr.V.Furman for fruitful discussions. Experimental investigations have been performed in collaboration with Mr.V.Khryachkov, Mr. V. Mitrofanov, Mrs.N.Semenova.

REFERENCES.

1. B.Rossi, H.Staub Ionization chambers and counters, McGraw -Hill, New York, 1979.
2. E.Segre ed. Experimental nuclear physics, V.I, 1952, John Wiley & Sons Inc, New York.
3. J.F.Ziegler, Handbook of stopping powers and ranges in all elemental matter, V.4 (Pergamon, New York, 1977).
4. O.Bunemann, T.E.Granshaw, J.A.Harvey, Can.J.Res. 27A (1949) 191.
5. A.A.Goverdovsky et.al. Report IPPE-2242, Obninsk, 1992.
6. Nuclear Standards File , INDC/NEANDC, 1981. IAEA, Vienna.
7. A.A.Goverdovsky et.al. Rad.Effects 93 (1986) 293.
8. J.B.Marion and F.C.Young Nuclear Reaction Analysis, Graphs and Tables, North Holland Publishing Co, Amsterdam, 1968.
9. M.Avrigeanu, M.Ivascu, V.Avrigeanu Z.Phys. A - Atomic Nuclei 335 (1989) 299.
10. C.Budtz-Jorgensen, H.-H. Knitter et.al. NIM A258 (1987) 209.
11. S.B.Kaufman, E.P.Steinberg, B.D.Wilkins et.al. NIM 115 (1974) 47.
12. E.L.Haines, A.B.Witehead Rev.Sci.Instr. 37 (1966) 190.

13. J.Lindhard, V.Nielsen, M.Scharff and P.V.Thomsen, K.Dan. Vidensk.Selsk.Mat.-Fys.Medd. 33 (1963) no.10.
14. J.Lindhard, M.Scharff and H.E.Schiott Ibid. 33 (1963) no.14.
15. P.T.Nielsen and N.Rud, University of Aarhus, private communication referred in [10].
16. A.A.Goverdovsky, V.F.Mitrofanov, V.A.Khrjachkov INDC(CCP) - 341, IAEA, Vienna (1991).
17. P.Moller and J.R.Nix At.Data Nucl.Data Tables 26 (1981) 165.
18. V.A.Khrjachkov, A.A.Goverdovsky, B.D.Kuzminov et.al. J.Nucl.Phys.(RUS) 53 N3 (1991) 621.
19. G.Simon et.al. NIM A286 (1990) 220.
20. Ch.Streade, thesis, Geel, Belgium, 1985.
21. E.E.Maslin, A.L.Rodgers and W.G.Core Phys.Rev. 164 N4 (1967) 1520.
22. J.W.Boldeman, A.R.de Musgrove, R.L.Walsh Austral.J.Phys. 24 N6 (1971) 821.
23. V.F.Apalin, Yu.N.Gritsyuk, I.E.Kutikov et.al. Nucl.Phys. 71 (1965) 553.
24. J.C.D.Milton and J.S.Fraser Can.J.Phys. 40 N11 (1962) 1626.
25. I.Kimura, Y.Nakagome and I.Kanno Proc. XVIIIth Int. Symp. Nucl. Phys., Gaussig, GDR, Nov. 1988. ZfK-732. P.29.
26. R.Muller, A.A.Naqvi, F.Kappeler, F.Dickman Phys.Rev. C29 (1984) 885.
27. H.W.Schmitt, J.H.Neiler and F.J.Walter Phys.Rev. 141 (1966) 1146.
28. A.A.Goverdovsky, V.F.Mitrofanov, V.A.Khrjachkov J.Nucl.Phys. (RUS) 1992, to be published.
29. H.-G.Clerc, W.Lang, M.Mutterer et.al. Nucl.Phys. A452 (1986) 277.
30. S.Bjornholm, J.E.Lynn Rev.Mod.Phys. 52 (1980) 725.
31. J.F. Berger, M.Girod and D.Gogny Nucl.Phys. A428 (1984) 23.
32. F.Gonnenwein, J,Kaufmann, W.Mollenkopf P.Geltenbort and A.Oed Proc.Int.Symp., Smolenice, CSFR, June 1991, to be published.
33. A.H.Wapstra and N.B.Gove Nucl.Data Tables 9 (1971) 265.
34. A.A.Goverdovsky and A.V.Ignatyuk Proc. XVIIIth Int. Symp. Nucl.Phys., Gaussig, GDR, Nov. 1988. ZfK. P.134.
35. A.V.Ignatyuk Statistical properties of excited atomic nuclei. Report INDC(CCP)-233/L , IAEA , Vienna. 1985.
36. D.Hilscher et.al. Proc. of the 3rd Adriatic Europhys. Conf. on Dynamics of Heavy-Ion Collisions, Hvar, Ygoslavia, 1981, p. 225.

37. A.Gavron et.al. Phys.Rev.Lett. 47 (1981) 1255; Phys.Rev. C35 (1987) 579; Phys.Lett. B176 (1986) 312.
38. W.P.Zank et.al. Phys.Rev. C33 (1986) 519.
39. D.J.Hinde et.al. Nucl.Phys. A452 (1986) 550.
40. D.Hilscher et.al. Proc. XVIIIth Int. Symp. Nucl. Phys., Gaussig, GDR, Nov. 1988. ZfK. P.304.
41. C.B.Franklyn Rad.Effects 93 N1 (1986) 323.
42. M.V.Blinov et.al. Sov. Phys. JETP 15 (1962) 704.
43. S.S.Kapoor et.al. Phys.Rev. 131 (1963) 283.
44. C.Budtz-Jorgensen and H.-H.Knitter Nucl. Phys. A490 (1988) 307.
45. U.Brosa and H.-H.Knitter Z. Phys. (1992) , to be published; and Proc.Int.Symp as in [40], P.145.
46. G.S.Boikov, V.D.Dmitriev, G.A.Kudyaev et.al. Sov.J.Nucl.Phys. 53 N3 (1991) 628 ; Z.Phys. 340 (1991) 79.
47. P.Koczon , Thesis, Darmstadt. 1987 .
48. P.Koczon et.al. Phys.Lett. B191 (1987) 249.
49. J.P.Theobald Preprint IKDA 86/6, TH Darmstadt 1986.
50. A.Bohr Proc. Int. Conf. peaceful Uses atom. Energy , Geneva, 1955. V.1. P.151 (1955).
51. J.R.Huizenga, A.N.Behkami and J.H.Roberts Proc.Int.Symp. Phys.Chem. of Fission, Vienna, 28 July-1 Aug. 1969. Vienna, IAEA, 1969, p.403.
52. E.P.Wigner Group Theory and its applacation to quantum mechanics of atomic spectra. Academic Press, New York, 1959.
53. J.A.Wheeler In: Fast Neutron Physics, Part II, Interscience Publishers, New York (1963) 2051.
54. A.Bohr and B.R.Mottelson Nuclear Structure, V.II, W.A. Benjamin, Inc- Reading, Massechusetts, U.S.A., 1975.
55. Yu.M.Chipenyuk, Yu.B.Ostapenko, G.N.Smirenkin, A.S.Soldatov Sov.J.Usp.Phys.Nauk 144 N 1 (1984) 3.
56. J.W.Meadows and C.Budtz-Jorgensen Report ANL/NDM - 64 (1982), ANL, U.S.A.
57. A.R.deMusgrove, J.W.Boldeman, J.L.Cook et.al. J.Phys. G: Nucl.Phys. 7 (1981) 549.
58. S.Ahmed, M.M.Islam, A.H.Khan et.al. Nucl.Sci.Engng 71 (1979) 208.
59. R.W.Lamphere Proc.Int.Symp. Phycs Chem. of Fission, IAEA, Vienna, 1965, V.1, p.63.
60. J.E.Simmons and R.L.Henkel Phys.Rev. 120 (1960) 198.
61. K.T.R.Davies, A.J.Sierk and J.R.Nix Phys.Rev. C13 (1976) 2385.

62. K.T.R.Davies et.al. Ibid. C16 (1977) 1890.
63. J.Blocki et.al. Ann.Phys. 113 (1978) 330.
64. J.R.Nix and A.J.Sierk Preprint LA-UR-86-698. Los Alamos. U.S.A. (1986).
65. G.D.Adeev, V.V.Pashkevich, N.I.Pischasov and O.I.Serdyuk Proc.Int.Symp.Nucl.Fission, Obninsk, USSR, July 1987 : Vopr. At.Nauki Tecniki, 1 (1988) 49.
66. F.Gonnenwein Ibid. p.14 ; Proc.Int.Symp. [40] but p.12.
67. A.A.Goverdovsky Report INDC(CCP)-307/L , IAEA, Vienna, 1989.
68. E.Aker Thesis, Karlsruhe, 1987.
69. R.W.Hasse Proc.Int.Symp. (Ref.[65]) p.3.
70. A.A.Goverdovsky et.al. Sov.J.Nucl.Phys. 44 (1986) 287 ; 46 (1987) 706 ; 48 (1988) 1251 ; 52 (1990) 1250.
71. A.A.Goverdovsky et.al. Proc.IAEA meeting, Mito-city, 1988. IAEA. Vienna. INDC(NDS)-220 (1989) p.59.